communications biology

A Nature Portfolio journal

Article

https://doi.org/10.1038/s42003-025-07958-4

OPN3-mediated positive regulation of angiogenesis in HUVECs through VEGFR2 interaction

Huanhuan Luo[1,2,3], Wei Zhang[2,3], Wen Zeng[2,3], Yu Wang[2,3], Jianglong Feng[2], Yinghua Lan[2], Xian Dong[2], Ting Liu[2], Yan Sun[2] & Hongguang Lu[1,2]

Many rhodopsin-like G-protein-coupled receptors (Rh-GPCRs) are known to either promote or inhibit angiogenesis. Among these, Opsin 4 and Opsin 5 are specifically involved in vascular development within the eye. Opsin 3 (OPN3), another member of Rh-GPCRs, performs a variety of light-dependent and light-independent functions in extraocular tissue. However, its role in endothelial cells and angiogenesis remains unclear. Here, we found that OPN3 knockdown or knockout in zebrafish impairs embryonic angiogenesis and vascular development. Similarly, silencing OPN3 in human umbilical vein endothelial cells (HUVECs) inhibits cellular proliferation, migration, sprouting, and tube formation, while OPN3 overexpression promotes these cellular processes. Moreover, OPN3 regulates angiogenesis in HUVECs through the VEGFR2-AKT pathway, with OPN3 and VEGFR2 co-localizing at the plasma membrane and forming a physical complex. These findings provide new insights into the non-light-dependent functions of OPN3 in angiogenesis, expanding our understanding of its physiological roles and offering potential therapeutic strategies for angiogenesis-related diseases.

Angiogenesis refers to the process of forming new blood vessels from existing capillaries, which involves the coordinated action of various cell types and signaling pathways, including endothelial cell activation, proliferation, migration, lumen formation, and maturation[1]. It plays a critical role in physiological processes such as embryonic development, wound healing, and tissue regeneration. However, abnormal angiogenesis can lead to diseases such as cancer and retinal disorders[2]. Therefore, a deeper understanding of angiogenesis mechanisms not only helps to reveal physiological phenomena but also provides new therapeutic targets[3]. VEGFR2 is a receptor tyrosine kinase (RTK) belonging to class IV of the vascular endothelial growth factor (VEGF) receptor family, expressed on endothelial cells, is central to angiogenesis. Its activation triggers downstream signaling pathways like PI3K/AKT and MAPK/ERK, promoting endothelial cell proliferation and migration[4,5].

Previous study demonstrated that G protein-coupled receptors (GPCRs) can regulate angiogenesis, with bidirectional activation between GPCRs and RTKs. The interaction between GPCRs and RTKs has become a target in drug development[6]. For example, G protein-coupled receptor 126 (GPR126) modulates VEGFR2 expression through STAT5 and GATA2, affecting physiological and pathological angiogenesis[7]. Thrombin, a GPCR agonist, stimulates VEGFR2 expression, influencing endothelial cell proliferation and migration[8]. VEGFR2 also interacts with the β2-adrenergic receptor in heteromeric complexes, affecting their localization and signaling within cells, with VEGF165a promoting VEGFR2 homodimerization[9]. Additionally, many Rh-GPCRs, which have negatively charged amino acid residues, facilitate ligand binding and support cell-cell interactions, playing crucial roles in angiogenesis[10]. Opsins (OPNs), belonging to subfamily A of the Rh-GPCR family, are involved in light-dependent angiogenesis[11,12]. UV light activates OPN5, leading to dopamine transporter (DAT) phosphorylation, which inhibits dopamine levels in the vitreous body. This suppresses VEGFR2 signaling, promoting normal regression of vitreous vessels. In OPN5 knockout models, dopamine levels rise, causing premature vascular degeneration[13]. OPN4 mediates light-dependent vascular development in the eye, controlling retinal cell structure and VEGFA levels. In OPN4 knockout mice or wild-type mice kept in darkness, vitreous vessels fail to regress, leading to excessive growth of retinal vessels[14]. OPN4 also regulates vascular function, particularly in light-induced relaxation, achieved through stimulation with specific wavelengths of light[15]. In pulmonary arteries, functional OPN3 and OPN4 represent an endogenous "optogenetic system" that mediates photorelaxation of the pulmonary vasculature. In OPN4$^{-/-}$ mice, the photorelaxation response is weakened, and further reduction in response is observed with shRNA-mediated knockdown of OPN3[16]. These findings suggest that OPN3 may regulate vascular endothelial cells (ECs) function and angiogenesis.

[1]School of Public Health, Guizhou Medical University, Guiyang, Guizhou, China. [2]Department of Dermatology, Affiliated Hospital of Guizhou Medical University, Guiyang, Guizhou, China. [3]These authors contributed equally: Huanhuan Luo, Wei Zhang, Wen Zeng, Yu Wang. e-mail: luhongguang@gmc.edu.cn

In this study, we investigated the role of OPN3 in ECs and angiogenesis using HUVECs. We found that OPN3 regulates angiogenesis by modulating cell proliferation, migration, and tube formation. OPN3 influences angiogenesis through the VEGFR2-mediated AKT pathway, and OPN3 and VEGFR2 form a physical complex in HUVECs. Additionally, OPN3 knockdown and knockout in zebrafish revealed that the absence of OPN3 significantly reduced the total length of embryonic blood vessels and vascular connections, while regulating VEGFR2 expression and AKT activation in vivo. These findings suggest new mechanisms in angiogenesis and potential therapeutic approaches for angiogenesis-related diseases.

Results

OPN3 is expressed in HUVECs and human dermal microvascular endothelial cells (HDMECs)

Vascular development is closely linked to the activation, proliferation, and migration of ECs[17]. To explore the role of OPN3 in ECs, we conducted immunohistochemistry on human normal skin and umbilical cord tissues. Using the CD31 antibody, an EC-specific marker[18], we confirmed vascular localization and found that OPN3 is expressed in the ECs of both tissue types (Fig. 1a, b). We further isolated HDMECs from human skin and cultured HUVECs from the umbilical vein. HUVECs were identified by immunofluorescence using CD31 and vWF markers (Fig. S1), while HDMECs were identified by flow cytometry using CD31 (Fig. S2), establishing a cellular model of vascular growth. Immunofluorescence analysis revealed OPN3 presence in ECs, localized to the cellular membrane and cytoplasm (Fig. 1c). We further assessed OPN3 expression in HUVECs and HDMECs using RT-qPCR and Western blot analyses, confirming its presence in HDMECs and HUVECs (Fig. 1d, e). These results suggest a potential functional role for OPN3 in human ECs in vitro.

OPN3 regulates cellular proliferation, migration, tube formation, and sprouting of HUVECs

To investigate the role of OPN3 in in vitro angiogenesis, we employed a previously reported method[19], infecting HUVECs with lentivirus to modulate intracellular *OPN3* expression. The transfection efficiency of puromycin-resistant cells was evaluated using fluorescence microscopy, revealing a transfection rate of nearly 100% (Fig. S3). RT-qPCR and Western blot analysis confirmed a substantial reduction in *OPN3* mRNA and OPN3 protein levels in cells treated with LV-OPN3-RNAi compared to the control group (LV-control-RNAi) (Fig. 2a, c). Conversely, in the OPN3 overexpression group (LV-OPN3), *OPN3* mRNA and OPN3 protein levels were significantly elevated compared to the control (LV-control) (Fig. 2b, d).

In the LV-OPN3-RNAi group, cell proliferation was notably reduced, with fewer cells observed compared to the LV-control-RNAi group. Microscopic examination revealed morphological changes: cells in the LV-control-RNAi group appeared elongated, spindle-shaped, or fusiform, exhibiting prominent pseudopodia and good extension. In contrast, cells in the LV-OPN3-RNAi group displayed a more rounded or irregular shape, fewer cell-cell connections, and poorer extension (Fig. 2e). Notably, no significant morphological changes were observed in the LV-OPN3 group compared to its control (Fig. 2f). A significant decrease in the proportion of EdU-positive nuclei was observed in the LV-OPN3-RNAi group, whereas the proportion increased in the LV-OPN3 group (Fig. 2g). Flow cytometry analysis further revealed an increased percentage of cells in the G1 phase and a decrease in the G2 and S phases in the LV-OPN3-RNAi group (Fig. 2h). In contrast, the LV-OPN3 group showed a reduced percentage of cells in the G1 phase and an increase in the G2 and S phases (Fig. 2h). These results collectively suggest that OPN3 expression influences HUVECs proliferation. In migration assays, the LV-OPN3-RNAi group demonstrated reduced cell migration, whereas the LV-OPN3 group showed enhanced migration (Fig. 2i). Similarly, tube formation assays revealed fewer tubular structures in the LV-OPN3-RNAi group and a significant increase in the LV-OPN3 group (Fig. 2j, k). In vitro sprouting experiments showed a marked reduction in both sprout number and total length in the LV-OPN3-RNAi group, while the LV-OPN3 group exhibited a significant increase in these parameters (Fig. 2l, m). Additionally, silencing *OPN3* expression in HDMECs using siRNA yielded results consistent with lentivirus-mediated *OPN3* knockdown in HUVECs (Fig. S4). These results further support the hypothesis that OPN3 can regulate proliferation, migration, tube formation, and sprouting in of human vascular endothelial cells.

To investigate the mechanisms by which OPN3 knockdown inhibits in vitro angiogenesis, we performed RNA-seq analysis on HUVECs with reduced *OPN3* expression. This analysis identified 2985 differentially expressed genes, of which 1379 were upregulated and 1606 were downregulated (Fig. 3a). Gene Ontology (GO) enrichment analysis revealed significant associations with pathways related to angiogenesis, blood vessel morphogenesis, and endothelial cell proliferation and migration (Fig. 3b). Furthermore, we observed a downregulation of *VEGFR2* (*KDR*) mRNA expression in the LV-OPN3-RNAi group (Fig. 3c), suggesting that OPN3 regulates endothelial function, at least in part, through VEGFR2 signaling.

OPN3 promotes proangiogenic effects in HUVECs by upregulating VEGFR2 expression

To investigate the relationship between OPN3 and VEGFR2 expression in HUVECs, we performed RT-qPCR and Western blot analyses. These assays confirmed that *VEGFR2* mRNA (Fig. 3d, e) and VEGFR2 protein levels (Fig. 4a, b) decreased following OPN3 knockdown. Confocal microscopy further revealed reduced VEGFR2 expression on the cell membrane and partial redistribution to the cytoplasm upon OPN3 silencing (Fig. S5a). Conversely, OPN3 overexpression increased *VEGFR2* mRNA and VEGFR2 protein levels (Fig. 4a, b) and enhanced VEGFR2 localization on the cell membrane (Fig. S5b).

To validate the role of VEGFR2, we silenced its expression using VEGFR2-RNAi, which was confirmed by RT-qPCR and Western blot (Fig. 4c, d). In HUVECs overexpressing OPN3, VEGFR2-RNAi significantly reduced tube formation and sprouting, effectively reversing the pro-angiogenic effects of OPN3 overexpression (Fig. 4f–h). Additionally, we observed that OPN3 expression levels were lower in the VEGFR2-RNAi group compared to the RNAi-control group (Fig. 4e), suggesting a potential mutual regulatory relationship between OPN3 and VEGFR2.

To further explore this regulatory interaction at the protein level, we overexpressed *OPN3* in the OPN3 knockdown group via plasmid transfection. Compared to the OPN3 knockdown group, the expression levels of both OPN3 and VEGFR2 were restored upon OPN3 overexpression (Fig. 5a, b). Conversely, in the OPN3 overexpression group, silencing *OPN3* using siRNA resulted in a significant downregulation of both OPN3 and VEGFR2 protein levels compared to the OPN3 overexpression group (Fig. 5c, d). These findings underscore a mutual regulatory relationship between OPN3 and VEGFR2, further highlighting their critical roles in angiogenesis.

OPN3 and VEGFR2 are able to form a complex

Given the regulatory relationship between OPN3 and VEGFR2, we hypothesized that they might form a functional or physical complex. To investigate this, we used confocal microscopy to examine the colocalization of endogenous OPN3 and VEGFR2 in HUVECs. The results showed partial colocalization of OPN3 and VEGFR2 in the plasma membrane and cytoplasm of HUVECs (Fig. S6a). Furthermore, co-immunoprecipitation (Co-IP) experiments confirmed their interaction. When HUVECs lysates were immunoprecipitated with an anti-VEGFR2 antibody and subsequently immunoblotted with an anti-OPN3 antibody, a band corresponding to the molecular weight of OPN3 was detected (Fig. S6b). To further explore the interaction at the molecular level, we utilized homology modeling and the HDOCK method to identify potential binding sites between OPN3 and VEGFR2[20]. Molecular docking simulations revealed that Ala690 of VEGFR2 forms a hydrogen bond with Arg73 of OPN3, while Ile669 of VEGFR2 interacts with Trp155 of OPN3 (Fig. S6c). These residues, located within the D7 domain of VEGFR2, are critical for its activation[21].

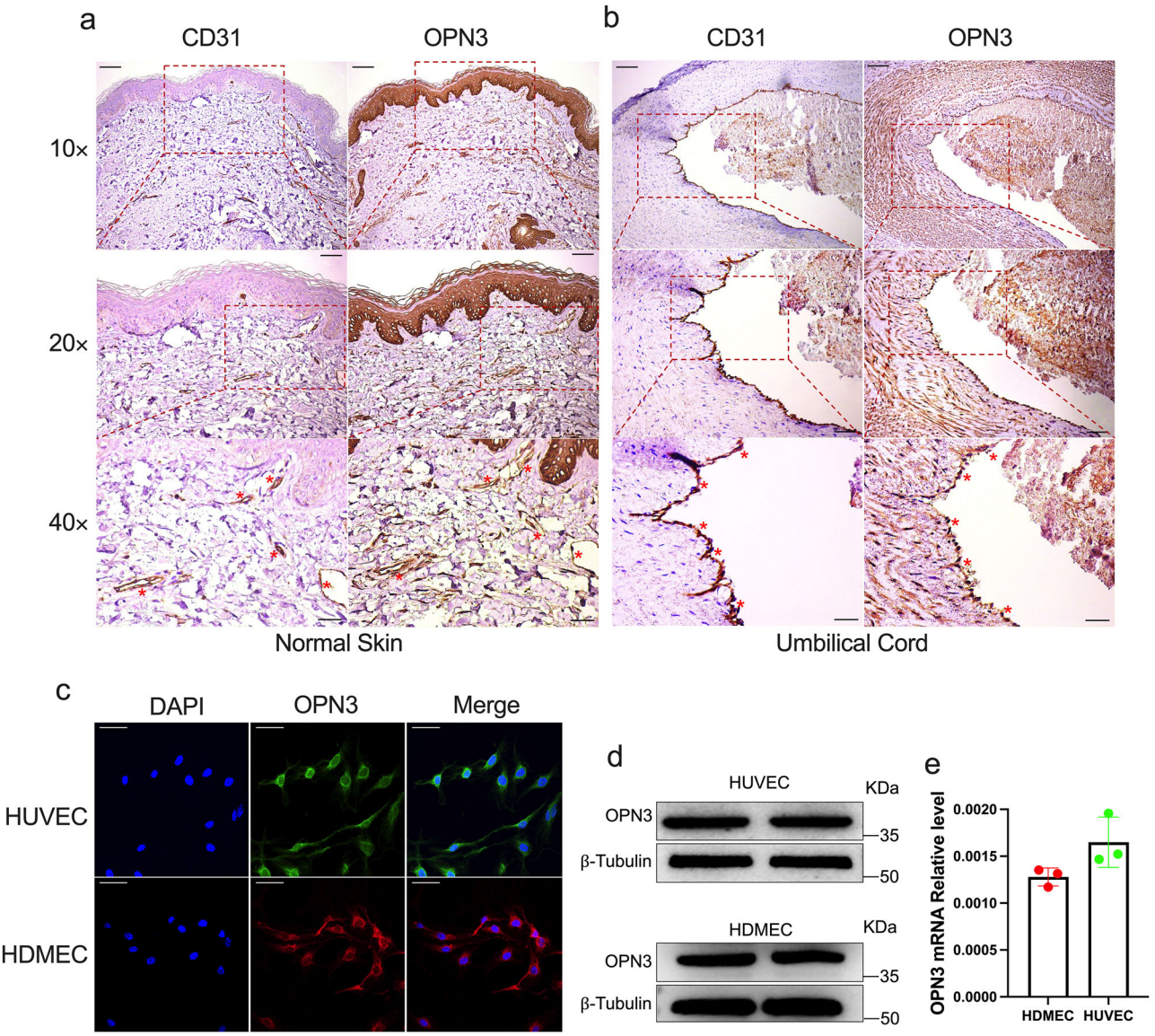

Fig. 1 | OPN3 expression in primary human vascular endothelial cells: HUVECs and HDMECs. a IHC staining of human skin tissue for CD31 and OPN3. CD31 positively marks dermal microvascular endothelial cells in human skin tissue, while OPN3 staining shows its expression in human skin, with higher expression observed in the basal layer of the epidermis. Comparing with the CD31-positive areas, OPN3-positive reactions were found in the same locations, indicating that OPN3 is expressed in HDMECs. The scale bar in the 10× panel corresponds to 100 μm, while the scale bar in the 20× panel represents 50 μm, and the scale bar in the 40× panel indicates 25 μm. Red asterisks indicate the locations of HDMECs. **b** IHC staining of human umbilical vein tissue for CD31 and OPN3. CD31 positively marks endothelial cells in the human umbilical vein tissue, while OPN3 staining shows its expression in the umbilical vein. Comparing with the CD31-positive areas, OPN3-positive reactions were found in the same locations, indicating that OPN3 is expressed in HUVECs. The scale bar in the 10× panel corresponds to 100 μm, while the scale bar in the 20× panel represents 50 μm, and the scale bar in the 40× panel indicates 25 μm. Red asterisks indicate the locations of HUVECs. **c** Laser confocal microscopy analysis of OPN3 protein expression and localization in HUVECs and HDMECs. Green indicates OPN3 in HUVECs, red indicates OPN3 in HDMECs, and blue represents the nucleus. The results show that OPN3 protein is mainly located on the plasma membrane. The scale bar represents 50 μm. **d** Western blot analysis of OPN3 protein expression in HDMECs and HUVECs, with β-tubulin used as a loading control for normalization of the WB analysis. **e** RT-qPCR analysis of *OPN3* mRNA expression in HDMECs and HUVECs. The relative mRNA expression levels were calculated using the $2^{-\Delta Ct}$ method, with *GAPDH* serving as the internal control ($n = 3$ independent experiments, with each experimental group consisting of 6 dishes, derived from 3 different donors, with each donor providing 2 dishes of cells).

VEGF can enhance the combination of OPN3 and VEGFR2

In angiogenesis, VEGFR2 activation-mediated signaling primarily depends on VEGF[22]. To further investigate this interaction, we stimulated HUVECs with 25 ng/mL VEGF. Co-IP analysis revealed that OPN3 weakly associates with VEGFR2 under basal conditions. However, this interaction is significantly enhanced after 15 min of VEGF stimulation and is sustained for at least 30 min (Fig. 5e, f). Confocal microscopy colocalization analysis further demonstrated that OPN3 is expressed on the cytoplasmic membrane and partially colocalizes with VEGFR2 under basal conditions. Following 15 min of VEGF stimulation, their colocalization on the membrane is markedly increased (Fig. 5g, h). These findings suggest that VEGF stimulation promotes the binding of OPN3 to VEGFR2 in HUVECs, thereby activating the VEGFR2 signaling pathway.

OPN3-induced proangiogenic effects are mediated by AKT activation

Our KEGG pathway enrichment analysis, based on RNA-seq results from HUVECs with reduced *OPN3* expression, revealed the involvement of the

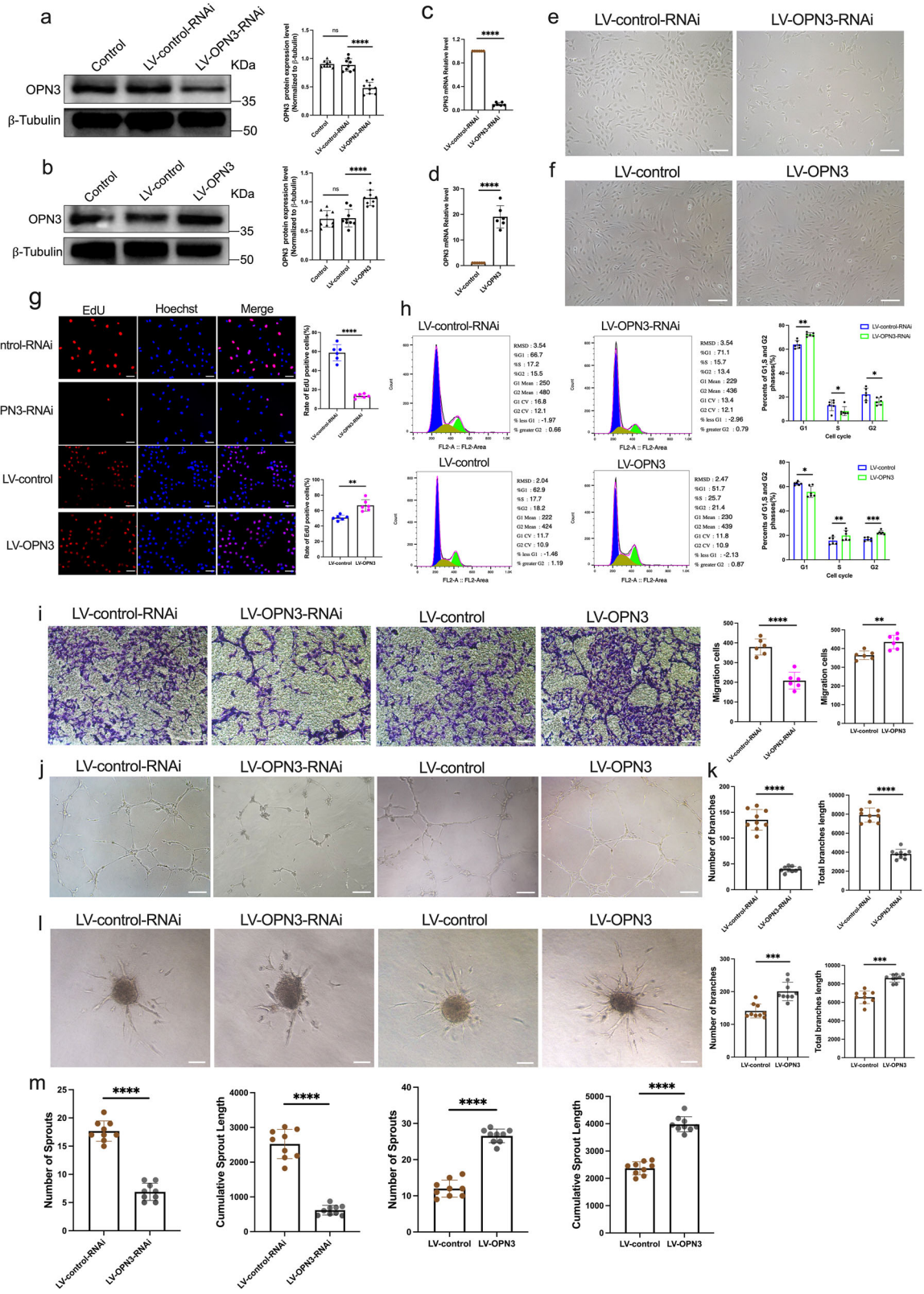

PI3K/AKT signaling pathway in angiogenesis (Fig. 6a). Activation of the AKT signaling axis in ECs plays a critical role in cardiovascular homeostasis and angiogenesis[23]. To investigate whether OPN3 is necessary for AKT activation in HUVECs, we performed functional assays. Silencing OPN3 inhibited AKT activation in HUVECs, while overexpression of OPN3 enhanced AKT phosphorylation (Fig. 6b, c).

To further demonstrate that AKT activation is essential for OPN3-mediated pro-angiogenic activity, we used MK-2206, a specific AKT inhibitor[24], to suppress AKT activation in OPN3-overexpressing HUVECs (Fig. 6d). Overexpression of OPN3 significantly promoted spheroid sprouting and tube formation, effects that were notably inhibited by MK-2206 (Fig. 6e, f). Conversely, we applied SC79, an AKT activator[25], to restore

Fig. 2 | The regulatory effects of OPN3 knockdown and overexpression on HUVECs proliferation, migration, tube formation and sprouting. In HUVECs, the *OPN3* knockdown cell model was constructed using LV-OPN3-RNAi lentivirus and the control LV-control-RNAi lentivirus. The *OPN3* overexpression cell model was constructed using LV-OPN3 and the control LV-control lentivirus, with the uninfected group serving as the Control. **a**, **b** The OPN3 protein levels were verified by Western blot, using β-tubulin as a loading control for normalization of the WB analysis. Relative protein levels were quantified using ImageJ software ($n = 9$ independent experiments, with each experimental group consisting of 18 dishes, derived from 9 different donors, with each donor providing 2 dishes of cells). Statistical analysis was performed using an unpaired t-test: ns: not significant, $^{****}p < 0.0001$. **c**, **d** The *OPN3* mRNA levels were verified by RT-qPCR. The relative mRNA expression levels were calculated using the $2^{-\Delta\Delta Ct}$ method, with *GAPDH* serving as the internal control ($n = 6$ independent experiments, with each experimental group consisting of 12 dishes, derived from 6 different donors, with each donor providing 2 dishes of cells). Statistical analysis was performed using an unpaired t-test: $^{****}p < 0.0001$. This analysis confirmed the successful construction of different experimental group cells. **e**, **f** After successful construction of the cell models, optical microscopy was used to observe the morphology and quantity of cells in different experimental groups. The scale bar represents 100 μm. **g** The cell proliferation was assessed by detecting the ratio of EdU-positive nuclei to total nuclei in different experimental groups. Blue Hoechst represents the total number of cells, while red represents EdU-positive cells. The counts of blue Hoechst and red EdU were analyzed using ImageJ software ($n = 6$ dishes of cultured HUVECs from 3 different donors, with each donor replicated twice). Statistical analysis was performed using an unpaired t-test: $^{**}p < 0.01$, $^{****}p < 0.0001$. The scale bar represents 50 μm. **h** The cell cycle in different experimental groups was analyzed by flow cytometry using FlowJo software ($n = 6$ independent experiments, with each experimental group consisting of 12 dishes, derived from 6 different donors, with each donor providing 2 dishes of cells). Statistical analysis was performed using an unpaired t-test: $^{*}p < 0.05$, $^{**}p < 0.01$, $^{***}p < 0.0001$. **i** The migration of cells in different experimental groups was assessed using the transwell assay, and images were captured under an optical microscope. The number of migrating cells was counted after staining with crystal violet, analyzed using ImageJ software ($n = 6$ dishes of cultured HUVECs from 3 different donors, with each donor replicated twice). Statistical analysis was performed using an unpaired t-test: $^{**}p < 0.01$, $^{****}p < 0.0001$. The scale bar represents 100 μm. **j**, **k** Cells from different experimental groups were seeded on Matrigel for 10 h to record and quantify the tube formation. The number and length of branches were analyzed using ImageJ software to determine the extent of tube formation ($n = 9$ dishes of cultured HUVECs from 3 different donors, with each donor replicated three times). Statistical analysis was performed using an unpaired t-test: $^{***}p < 0.001$, $^{****}p < 0.0001$. The scale bar represents 100 μm. **l**, **m** Spheroid sprouting experiments were conducted with cells from different experimental groups. The sprouts were recorded and quantified using optical microscopy, and the number and length of sprouts were analyzed using ImageJ software to evaluate the sprouting ability of ECs ($n = 9$ dishes of cultured HUVECs from 3 different donors, with each donor replicated three times). Statistical analysis was performed using an unpaired t-test: $^{****}p < 0.0001$. The scale bar represents 100 μm. Data are presented as mean ± SEM.

AKT activity in OPN3-knockdown HUVECs (Fig. 6g). The impairment of spheroid sprouting and tube formation caused by OPN3 knockdown was effectively rescued by SC79 (Fig. 6h, i). In addition, we observed that VEGF stimulation for 15 min enhanced p-AKT expression in HUVECs (Fig. S7a). To determine whether VEGF-induced AKT activation is dependent on OPN3, we stimulated OPN3-knockdown HUVECs with VEGF. The results showed that OPN3 knockdown reduced VEGF-induced AKT activation (Fig. S7b). These findings indicate that OPN3 exerts its pro-angiogenic effects in HUVECs by enhancing AKT activation and that OPN3 is a critical mediator of VEGF-induced AKT activation in HUVECs.

Silencing or knockout of OPN3 causes angiogenesis deficiency during embryogenesis

Zebrafish are ideal models for studying vascular development due to their transparent embryos, rapid development, genetic tractability, and high physiological similarity to mammals[26]. A Basic Local Alignment Search Tool (BLAST) analysis of the National Center for Biotechnology Information (NCBI) database revealed a 61.79% homology between human and zebrafish OPN3, supporting the relevance of zebrafish in studying OPN3's function.

In our study, we utilized transgenic *fli1*:EGFP zebrafish, which express enhanced green fluorescent protein (EGFP) in ECs[27], to investigate the role of OPN3 in angiogenesis. To achieve targeted gene knockdown, we microinjected single-cell-stage embryos with either Control Morpholino (MO) or OPN3 MO. At 48 h post-fertilization (hpf), western blot analysis confirmed effective knockdown of OPN3 protein levels following OPN3 MO injection, with partial restoration upon co-injection with in vitro transcribed OPN3 mRNA (Fig. 7b). Confocal microscopy revealed that OPN3 knockdown led to a significant reduction in blood vessel length, diminished vascular connections, and defects in dorsal anastomotic vessel (DAV) fusion. Notably, co-injection of OPN3 mRNA successfully rescued these vascular defects, confirming the critical role of OPN3 in vascular development (Fig. 7a).

To further validate these findings, we employed CRISPR/Cas9 genome editing to generate zebrafish with complete OPN3 knockout (*OPN3*$^{-/-}$). A mutant allele containing a + 111 bp insertion causing a frameshift and premature stop codon was selected for subsequent analyses. Western blot analysis confirmed the depletion of OPN3 protein expression in *OPN3*$^{-/-}$ mutants (Fig. 7d). Homozygous F2 *OPN3*$^{-/-}$ mutants were examined at key developmental time points (24 hpf, 48 hpf, and 72 hpf). Confocal imaging revealed significant vascular development defects, including reduced vascular length, junction density, and abnormal vascular morphogenesis in both the brain and trunk regions of *OPN3*$^{-/-}$ embryos (Fig. 7c, e). These complementary knockdown and knockout approaches conclusively demonstrate that OPN3 is indispensable for normal vascular development in zebrafish.

OPN3 regulates VEGFR2 expression and AKT activation in vivo

To verify whether OPN3 regulates VEGFR2 expression in vivo in zebrafish, we conducted Western blot analysis to measure OPN3 and VEGFR2 protein levels in *fli1*:EGFP zebrafish embryos with OPN3 knockdown (OPN3 MO) and OPN3 knockout (*OPN3*$^{-/-}$). The results demonstrated that depletion of OPN3 significantly reduced VEGFR2 protein expression in vivo (Fig. 8a, b).

In Tg(*kdrl*:mCherry) zebrafish, the kdrl promoter drives mCherry expression, serving as an indicator of VEGFR2 levels[28]. To further investigate the role of OPN3 in regulating VEGFR2 expression in vivo, single-cell stage embryos were injected with either a control morpholino (control MO) or an OPN3-targeting morpholino (OPN3 MO). At 48 hpf, Western blot analysis was performed. The results revealed a significant reduction in VEGFR2 protein levels following OPN3 knockdown. Importantly, co-injection of OPN3 MO with OPN3 mRNA partially restored VEGFR2 protein levels (Fig. 8c). Confocal microscopy also demonstrated a significant decrease in mCherry fluorescence intensity in embryos injected with OPN3 MO, which was effectively rescued by co-injection of OPN3 mRNA (Fig. 8d, e). These findings corroborated the western blot results (Fig. 8c). Taken together, these in vivo findings indicate that OPN3 knockdown leads to a reduction in VEGFR2 expression, which can be rescued by exogenous OPN3 mRNA. These results provide consistent evidence that OPN3 positively regulates VEGFR2 expression both in vivo and in vitro.

Furthermore, to evaluate whether OPN3 regulates the downstream signaling of VEGFR2, specifically AKT phosphorylation (p-AKT). In vivo, we examined p-AKT levels in embryos with OPN3 knockdown. We co-injected OPN3-MO and the AKT activator SC79 into *fli1*:EGFP zebrafish embryos. p-AKT expression was reduced in OPN3-knockdown embryos, but its expression was saved after SC79 injection (Fig. 8h, i). Moreover, this co-injection partially rescued the angiogenesis defects caused by OPN3 knockdown (Fig. 8f, g). These in vivo findings indicate that OPN3 influences VEGFR2-mediated AKT activation and plays a critical role in the regulation of angiogenesis.

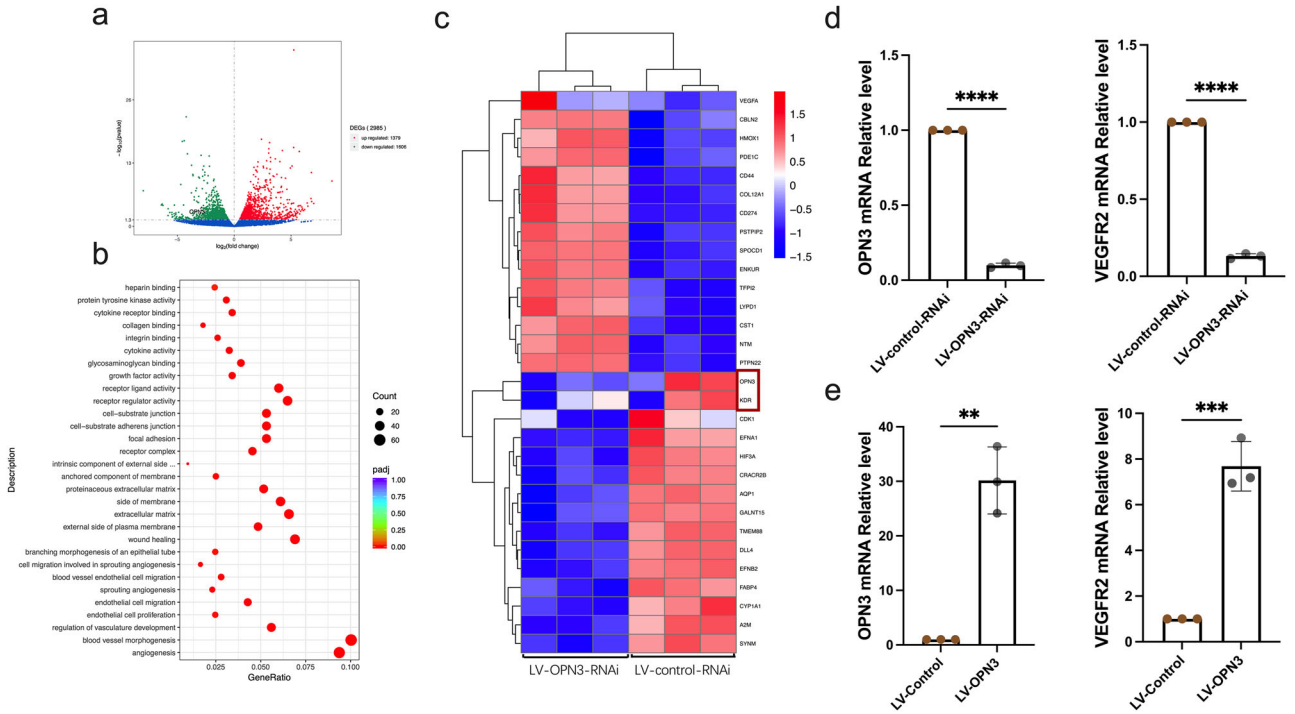

Fig. 3 | OPN3-deficient attenuates HUVECs angiogenesis. a The volcano plot of differentially expressed genes based on transcriptome sequencing results shows the fold change of gene expression (log2FoldChange) on the horizontal axis, representing the expression fold change between the LV-OPN3-RNAi and LV-control-RNAi. The vertical axis represents the significance level of the gene expression difference between the two groups (-log10pvalue). Red dots indicate upregulated genes, while green dots indicate downregulated genes. **b** The scatter plot of GO functional enrichment analysis based on transcriptome sequencing results is divided into three categories: biological process, cellular component, and molecular function. A total of 30 significant terms are selected from the GO enrichment analysis results for visualization, with a threshold of *padj* < *0.05* to define significant enrichment. The horizontal axis represents the ratio of the number of differentially expressed genes annotated to the GO term to the total number of differentially expressed genes. The vertical axis represents the GO terms. The size of the dots corresponds to the number of genes annotated to the GO term, and the color gradient from red to purple reflects the significance of enrichment. **c** Based on the transcriptome sequencing results, hierarchical clustering was performed on the FPKM values of the genes, and the row (genes) was normalized (Z-score). The resulting heatmap clusters genes with similar expression patterns together. In the heatmap, the colors represent the expression levels of the same gene across different samples, and each square's color reflects the normalized expression value (ranging from −1.5 to 1.5). Red indicates higher expression, and blue indicates lower expression. **d**, **e** RT-qPCR was used to detect the mRNA expression levels of *OPN3* and *VEGFR2* after *OPN3* knockdown and overexpression in HUVECs. The relative mRNA expression levels were calculated using the $2^{-\Delta\Delta Ct}$ method, with *GAPDH* serving as the internal control ($n = 3$ independent experiments, with each experimental group consisting of 6 dishes, derived from 3 different donors, with each donor providing 2 dishes of cells). Statistical analysis was performed using an unpaired t-test: $^{**}p < 0.01$, $^{***}p < 0.001$, $^{****}p < 0.0001$.

Discussion

In this study, we explored the role of OPN3 in angiogenesis, particularly its regulatory function in the VEGFR2 signaling pathway. Using zebrafish models and in vitro experiments with HUVECs, we found that the expression of OPN3 in ECs is crucial for angiogenesis. The loss of OPN3 significantly reduced HUVECs proliferation, migration, and tube formation abilities, leading to vascular developmental defects in zebrafish embryos. Additionally, Co-IP analysis confirmed the interaction between OPN3 and VEGFR2, and molecular docking models predicted their binding patterns, further supporting the conclusion of OPN3-VEGFR2 binding. We also confirmed that OPN3 promotes angiogenesis by regulating VEGFR2 activation and downstream AKT signaling. These findings validate the role of endothelial-specific Rh-GPCRs in positively regulating angiogenesis and provide important insights for various biological fields, including vascular development, tissue repair, and tumor progression.

Angiogenesis is essential for physiological and pathological processes such as embryo development, tissue repair, and tumor progression. In healthy tissues, angiogenesis aids organ development, wound healing, and tissue regeneration. However, in pathological conditions like cancer, diabetic retinopathy, and cardiovascular diseases, abnormal angiogenesis may contribute to disease onset and progression[2,29,30]. Angiogenesis is regulated by various molecules and signaling pathways, among which VEGF and its receptors play a central role.

VEGF receptors (VEGFRs) belong to the receptor tyrosine kinase family and mainly include VEGFR1, VEGFR2, and VEGFR3. VEGFR1 and VEGFR2 are primarily expressed in ECs, while VEGFR3 is mainly involved in lymphatic vessel development and function regulation[31]. VEGFR1 and VEGFR2 share similar structures, including seven transmembrane helices, an extracellular ligand-binding region, and an intracellular kinase domain. Despite their structural similarities, they differ significantly in function and regulatory mechanisms[32]. VEGFR1 has a dual role: it inhibits embryonic angiogenesis by binding to VEGFA, while also exerting positive regulatory effects through tyrosine kinase-dependent signaling in adult tissues. Although VEGFR1 has a high affinity for VEGF, it shows lower activity in cultured cells, and only weak responses in ECs proliferation, migration, and tube formation are observed even in cells overexpressing VEGFR1. Despite self-phosphorylation of multiple tyrosine residues in response to VEGFA stimulation, this phosphorylation typically results in weak responses in endothelial cells[33–35]. In contrast, VEGFR2 serves as the main positive signal sensor for physiological and pathological angiogenesis. Its activation directly promotes ECs proliferation, migration, tube formation, and various stages of angiogenesis through multiple downstream signaling pathways, such as PI3K/AKT and MAPK. VEGFR2 is especially crucial in the formation and extension of new blood vessels[4,35].

Previous studies have emphasized the critical role of GPCRs and VEGFR2 in angiogenesis, but their interaction with photoreceptors has been

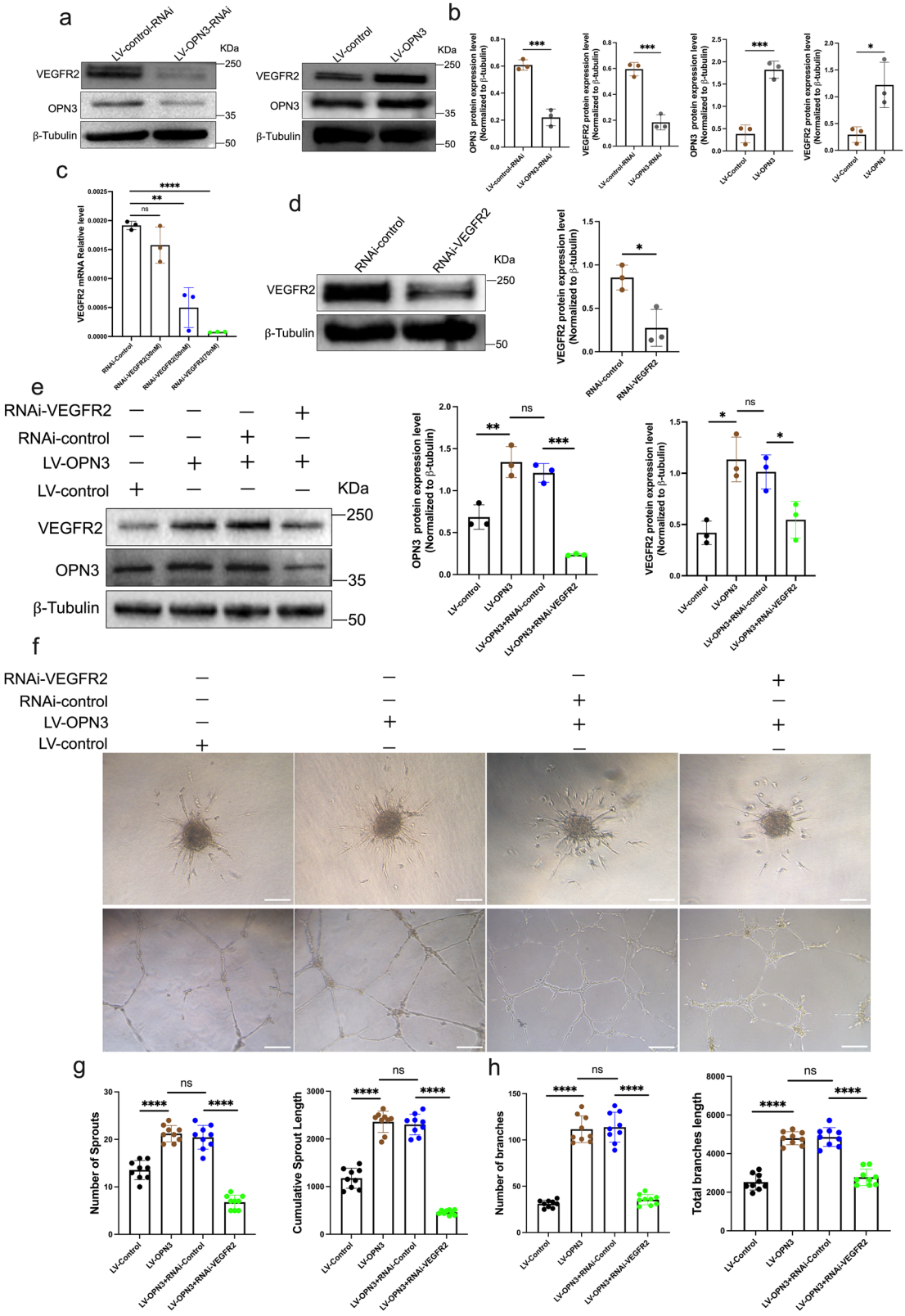

relatively underexplored. Research indicates that OPN4 regulates eye vascular development by influencing VEGFA expression. We hypothesized that OPN3 might affect VEGFR2 function by regulating VEGFA expression[14]. However, through RNA-seq differential gene analysis, we found that VEGFA levels increased in OPN3-knockdown HUVECs, while VEGFR2 expression was significantly reduced compared to the control group (Fig. 3c). Combining this with previous reports showing that OPN5 affects VEGFR2 expression and mediates vitreous vascular regression[13]. In this study, we found that OPN3 not only regulates the expression of VEGFR2, but VEGFR2 can also regulate the expression of OPN3, thereby affecting the function of HUVECs. This indicates that OPN3 and VEGFR2 can interact functionally. Studies have shown that OPN3 co-localizes with

Fig. 4 | OPN3-induced proangiogenic in HUVECs is mediated by promoting VEGFR2 expression. a, **b** Western blot analysis was used to detect the protein expression of OPN3 and VEGFR2 after lentiviral knockdown and overexpression of OPN3, using β-tubulin as a loading control for normalization in the WB analysis. Relative protein levels were quantified using ImageJ software ($n = 3$ independent experiments, with each experimental group consisting of 6 dishes, derived from 3 different donors, with each donor providing 2 dishes of cells). Statistical analysis was performed using an unpaired t-test: ns (not significant), $^{*}p < 0.05$, $^{***}p < 0.001$. **c** SiRNA was used to silence *VEGFR2* expression in HUVECs. The experiment was divided into a knockdown group (RNAi-VEGFR2) and a control group (RNAi-control). RT-qPCR was used to detect the mRNA expression levels of *VEGFR2* under different siRNA concentrations (30 nM, 50 nM, 70 nM). The relative mRNA expression levels were calculated using the $2^{-\Delta\Delta Ct}$ method, with *GAPDH* serving as the internal control ($n = 3$ independent experiments, with each experimental group consisting of 6 dishes, derived from 3 different donors, with each donor providing 2 dishes of cells). Statistical analysis was performed using an unpaired t-test: ns (not significant), $^{**}p < 0.01$, $^{****}p < 0.0001$. **d** Western blot analysis was used to detect VEGFR2 protein expression under 50 nM siRNA treatment, using β-tubulin as a loading control for normalization in the WB analysis. Relative protein levels were quantified using ImageJ software ($n = 3$ independent experiments, with each experimental group consisting of 6 dishes, derived from 3 different donors, with each donor providing 2 dishes of cells). Statistical analysis was performed using an unpaired t-test: $^{*}p < 0.05$. **e** Western blot analysis was used to detect OPN3 and VEGFR2 protein expression levels in different cell groups with overexpression of OPN3 or simultaneous overexpression of OPN3 and knockdown of VEGFR2, using β-tubulin as a loading control for normalization in the WB analysis. Relative protein levels were quantified using ImageJ software ($n = 3$ independent experiments, with each experimental group consisting of 6 dishes, derived from 3 different donors, with each donor providing 2 dishes of cells). Statistical analysis was performed using an unpaired t-test: ns (not significant), $^{*}p < 0.05$, $^{**}p < 0.01$, $^{***}p < 0.001$. **f**, **h** Cells from different experimental groups were seeded on Matrigel for 10 h to record and quantify tube formation. The number and length of branches were analyzed using ImageJ software to determine the extent of tube formation. **f**, **g** Spheroid sprouting experiments were conducted with cells from different experimental groups. The sprouts were recorded and quantified using optical microscopy, and the number and length of sprouts were analyzed using ImageJ software to evaluate the sprouting ability of HUVECs ($n = 9$ dishes of cultured HUVECs from 3 different donors, with each donor replicated three times). Statistical analysis was performed using an unpaired t-test: ns (not significant), $^{****}p < 0.0001$. The scale bar represents 100 μm. Data are presented as mean ± SEM.

MC1R in the plasma membrane and intracellular structures to form a physical complex[36]. OPN3 and MC4R can form a molecular complex[37]. OPN3 also seems to form a physical complex with BRAF V600E[38]. Based on these reports, we demonstrate here that OPN3 in ECs interacts with VEGFR2 to form a physical complex. This interaction is dynamically regulated within the cell, and after VEGF stimulation, the co-localization of OPN3 and VEGFR2 significantly increases, further confirming the functional link between them. Molecular docking analysis shows that the binding between OPN3 and VEGFR2 involves two hydrogen bonds: one between the side chain of Arg73 in OPN3 and the main chain carbonyl of Ala690 in VEGFR2, and another between the side chain of Trp155 in OPN3 and the main chain carbonyl of Ile669 in VEGFR2.

Ile669 and Ala690 are located in the seventh immunoglobulin-like domain (D7) of VEGFR2's protein kinase domain, which is closest to the cell membrane[21]. It is known that D7 stabilizes the active conformation of the kinase domain, promoting VEGFR2 autophosphorylation and regulating its kinase activity and angiogenesis[39]. Mutations or alterations in these amino acid residues may impair VEGFR2 activity[40]. VEGFR2 is capable of forming dimers, and this dimerization is critical for its activation and downstream signal transduction. Studies have shown that VEGFR2 can undergo ligand-independent dimerization, and the dimerized receptors can still initiate signaling by phosphorylating specific tyrosine residues, thereby activating a series of downstream signaling pathways[41,42]. The D7 domain is essential for forming properly oriented VEGFR2 dimers and stabilizing the unliganded VEGFR2 dimer[40]. Therefore, future studies need to characterize the role of OPN3 binding to VEGFR2 in the dimerization process.

In this study, we also observed that when OPN3 expression was knocked down, in addition to a reduction in the cell membrane expression of VEGFR2, some of the VEGFR2 accumulated in the cytoplasm (Fig. S5). Thus, the complex formed between OPN3 and VEGFR2 may also affect the stability of the receptor on the plasma membrane. Similar to the interaction between MC1R and OPN3[36], the OPN3-VEGFR2 complex might change the trafficking of VEGFR2 to and from the plasma membrane, thereby affecting its function. In addition to the direct interaction between OPN3 and VEGFR2, we also propose that OPN3 may modulate VEGFR2 signaling through G protein signaling pathways, particularly via Gαi. In mosquitoes, OPN3 has been shown to couple with the G protein Gαi/o subunit[43]. This mechanism has been previously confirmed in the interaction between OPN3 and MC1R, where OPN3 modulates the receptor's cAMP response via Gαi[36]. OPN3 also bidirectionally regulated the MC4R-activated cAMP response in a Gαi/o-dependent manner[37]. Similarly, we hypothesize that OPN3 can influence VEGFR2 signaling by altering its coupling with Gαi, which is known to play a role in regulating angiogenesis and endothelial cell behavior. This is particularly relevant to VEGFR2 internalization and downstream signaling[44]. Studies have reported that Gαi1/3 is part of the VEGFR2 internalization complex (VEGFR2-Ephrin-B2-Dab2-PAR-3), and it is essential for VEGFR2 internalization and downstream signaling. Knockdown, knockout, or mutation of Gαi1/3 inhibits VEGF-induced VEGFR2 internalization, as well as downstream AKT-mTOR and ERK-MAPK activation, and VEGF-induced angiogenesis both in vitro and in vivo, as well as HUVEC proliferation, migration, invasion, and tube formation[45]. Therefore, OPN3 may modulate VEGFR2 and Gαi interactions, altering downstream signaling cascades and angiogenesis, which will be determined by future research.

Arg73 and Trp155 are located in the transmembrane helices 2 (TM2) and 4 (TM4) of OPN3, respectively. These residues likely play a crucial role in retinal binding, light absorption, and initiating photoreceptor responses[46–49]. Given that OPN3 is a light-sensitive GPCR protein, it may regulate ECs function through various signaling pathways upon light exposure.

Previous studies have reported that blue light radiation can promote angiogenesis and accelerate wound healing in ischemic flap models[50]. OPN3 can sense blue light, with its absorption peak within the blue light range[43,51], which is closely associated with wound healing[52]. Additionally, blue light regulates melanogenesis in melanocytes through OPN3-dependent photoreceptor activation[53]. When we irradiated HUVECs and HDMECs with blue light, we observed a significant upregulation of OPN3 expression at doses of 7–14 J/cm^2 (Figure S9a, b). Subsequently, under 14 J/cm^2 blue light irradiation, we assessed ECs proliferation, migration, tube formation, and spheroid sprouting, and found enhanced cellular functions (Figure S9c–h). However, when OPN3 was knocked down in HUVECs, blue light irradiation resulted in reduced tube formation and spheroid sprouting (Figure S9i–l). We then measured VEGFR2 expression and found that it was upregulated with increased OPN3 expression under 14 J/cm^2 blue light irradiation (Figure S9m, n). These results suggest that the pro-angiogenic effect of blue light in HUVECs might be mediated through OPN3-regulated VEGFR2 expression. However, whether blue light further enhances the interaction between OPN3 and VEGFR2, thereby accelerating the angiogenesis process, requires further investigation.

In conclusion, this study demonstrates that OPN3 plays a key role in angiogenesis by interacting with VEGFR2 to regulate AKT activity. These findings enrich our understanding of the regulatory mechanisms of Rh-GPCRs in angiogenesis. Our research provides not only new insights for basic research but also potential targets for the treatment of vascular-related diseases. Future studies could further explore the role of OPN3 under various pathological conditions and assess its feasibility as a therapeutic target.

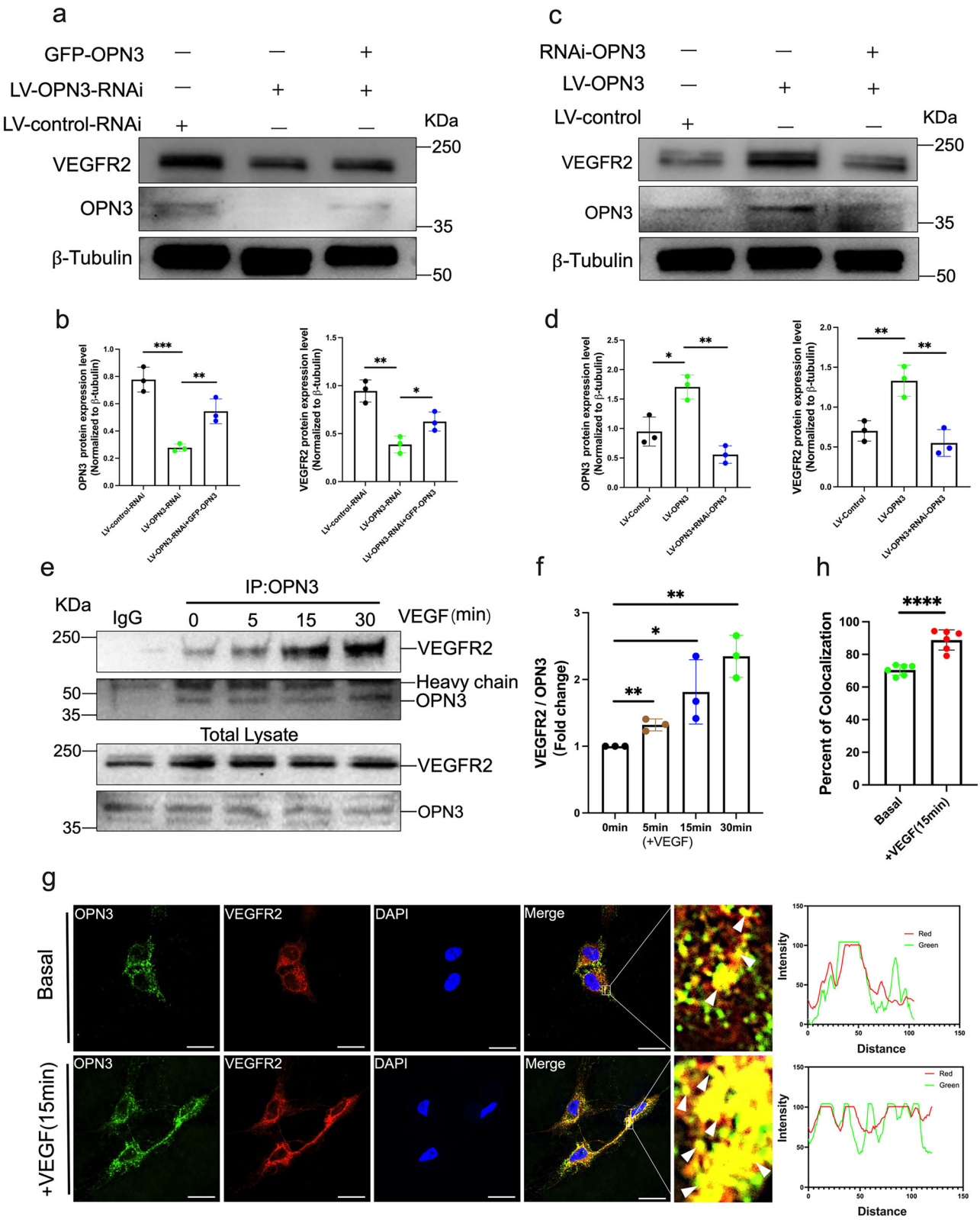

Materials and methods

Human samples

Human skin tissues were obtained from discarded foreskin samples following circumcision of healthy male donors aged 20–40 years. These samples were provided by the Department of Urology at the Affiliated Hospital of Guizhou Medical University. Human umbilical cord tissues were collected from normal umbilical cord samples discarded after cesarean sections performed on healthy female donors aged 20–35 years, from the Obstetrics Department of the same hospital. All ethical regulations relevant to human research participants were followed. Written informed consent was obtained from all volunteers or their legal guardians. The study was approved by the Ethics Committee of the Affiliated Hospital of Guizhou Medical University (Approval: #2021-541; #2023-740). This research was conducted in accordance with the principles outlined in the Declaration of

Fig. 5 | OPN3 and VEGFR2 are able to form a complex. a, **b** Western blot analysis was used to detect the protein levels of OPN3 and VEGFR2 in different cell groups with lentiviral knockdown of *OPN3* or lentiviral knockdown of *OPN3* combined with plasmid overexpression of *OPN3* (GFP-OPN3), using β-tubulin as a loading control for normalization in the WB analysis. Relative protein levels were quantified using ImageJ software ($n = 3$ independent experiments, with each experimental group consisting of 6 dishes, derived from 3 different donors, with each donor providing 2 dishes of cells). Statistical analysis was performed using an unpaired t-test: ns (not significant), $^{*}p < 0.05$, $^{**}p < 0.01$, $^{***}p < 0.001$. **c**, **d** Western blot analysis was used to detect the protein levels of OPN3 and VEGFR2 in different cell groups with lentiviral overexpression of *OPN3* or overexpression of *OPN3* combined with siRNA-mediated knockdown of *OPN3* (RNAi-OPN3), using β-tubulin as a loading control for normalization in the WB analysis. Relative protein levels were quantified using ImageJ software ($n = 3$ independent experiments, with each experimental group consisting of 6 dishes, derived from 3 different donors, with each donor providing 2 dishes of cells). Statistical analysis was performed using an unpaired t-test: $^{*}p < 0.05$, $^{**}p < 0.01$. **e** HUVECs were stimulated with VEGF (25 ng/mL), and cells were collected at different time points (5 min, 15 min, 30 min) to detect the interaction between OPN3 and VEGFR2 by Co-IP. Anti-OPN3 or anti-IgG (negative control) antibodies were used for immunoprecipitation (IP), followed by western blot analysis to detect OPN3 and VEGFR2 protein levels. Relative protein levels were quantified using ImageJ software. **f** Bar graph represents the averaged fold change of VEGFR2/OPN3 ratio over the basal ratio ($n = 3$ independent experiments, with each experimental group consisting of 12 dishes, derived from 6 different donors, with each donor providing 2 dishes of cells). Statistical analysis was performed using an unpaired t-test: $^{*}p < 0.05$, $^{**}p < 0.01$. **g**, **h** HUVECs were stimulated or not stimulated with VEGF for 15 min, followed by co-staining of OPN3 and VEGFR2. Images were captured using confocal microscopy. OPN3 was labeled in green, VEGFR2 in red, and DAPI in blue. The scale bar represents 25 μm. Yellow fluorescence (indicated by white arrows) in the merged images indicates their colocalization, which was analyzed by comparing the fluorescence intensity of each protein along the white line in the magnified images of the white box. A bar graph shows the percentage of colocalization ($n = 6$ dishes of cultured HUVECs from 3 different donors, with each donor replicated twice). Statistical analysis was performed using an unpaired t-test: $^{***}p < 0.001$.

Helsinki and the International Ethical Guidelines for Health-Related Research Involving Humans.

Immunohistochemical

Tissue sections were fixed overnight in 4% formaldehyde (P1110, Solarbio, China) and subsequently embedded in paraffin. Three-micrometer sections were deparaffinized, rehydrated, and subjected to antigen retrieval using an EDTA-based solution (ZLI-9069, ZSGB-BIO, China). Endogenous peroxidase activity was blocked with 3% hydrogen peroxide (PV-9000; ZSGB-BIO, China), and non-specific binding was blocked by incubating with 5% goat serum (ZLI-9056, ZSGB-BIO, China). Sections were incubated overnight with primary antibodies against OPN3 (ab228748, Rabbit, 1:800, Abcam, UK) and CD31 (ab9498, Mouse, 1:1000, Abcam, UK), followed by incubation with the secondary antibody (PV9000, ZSGB-BIO, China) at 37 °C for 30 min. Detection was performed using DAB (ZLI9018, ZSGB-BIO, China), and the sections were counterstained with hematoxylin.

Cell culture

Based on previous research methods[54], human umbilical vein endothelial cells (HUVECs) were isolated from the umbilical cord. To begin, 15 mL of type I collagenase (C8140, Solarbio, China) was injected into the umbilical vein, followed by digestion at 37 °C for 30 min. The reaction was then terminated by adding fetal bovine serum (FBS, FBSST-01033-500, OriCell, China), and the cells were collected by centrifugation. The isolated cells were cultured in endothelial cell medium (ECM, ScienCell, USA) supplemented with 5% FBS (0025, ScienCell, USA), 0.5% endothelial cell growth supplement (ECGS, 1052, ScienCell, USA), and 0.5% antibiotic solution (P/S, 0503, ScienCell, USA).

Human dermal microvascular endothelial cells (HDMECs) were isolated from post-surgical skin tissue. The skin flaps were digested with Dispase II (SCM133, Sigma, Germany) at 37 °C for 90 min to separate the epidermis, after which the dermis was further digested with type I collagenase (SCR103, Sigma, Germany) at 37 °C for 40 min. The reaction was then halted by the addition of FBS (FBSST-01033-500, OriCell, China). The digested tissue was filtered through a 40 μm filter (F8200, Solarbio, China), and the cells were resuspended in ECM. They were seeded into gelatin-coated culture dishes (G0040, Solarbio, China) and incubated at 37 °C with 5% CO_2. After 8 days, the cells underwent magnetic bead sorting using the CD31 MicroBead Kit (130-091-935, Miltenyi, Germany), following the manufacturer's instructions. A second round of sorting was performed 4 days later to further enrich the population of ECs.

Immunofluorescence staining

According to the manufacturer's instructions (abs50012, Absin, China), HUVECs and HDMECs were seeded at a density of 1.0×10^4 cells per well in confocal dishes and incubated at 37 °C with 5% CO_2 for 24 h. The cells were then fixed with 4% paraformaldehyde for 10 min, air-dried, and blocked with 5% goat serum for 30 min at 37 °C. After blocking, the cells were washed with PBS and incubated overnight at 4 °C with primary antibodies targeting vWF (AF3000, Rabbit, 1:500, AffBiotech, USA), CD31 (ab9498, Mouse, 1:1000, Abcam, UK), OPN3 (ab75285, Rabbit, 1:800, Abcam, UK), and VEGFR2 (55B11, Rabbit, 1:1000, Cell Signaling Technology, USA). The next day, after three washes with PBS, the cells were incubated with HRP-conjugated secondary antibodies (abs50012, Absin, China) for 45 min at 37 °C. Following another round of PBS washed, fluorescent staining was performed using TSA Fluorescein 520 or TSA Rhodamine 570 dyes (1:100) for 30 min. Finally, nuclei were counterstained with 4′,6-diamidino-2-phenylindole (DAPI, D9542, Sigma-Aldrich) for 10 min at room temperature.

Real-time quantitative PCR

Total RNA was extracted from cells using the TRIzol reagent (15596018, Invitrogen, USA) according to the manufacturer's instructions. The extracted RNA was then reverse transcribed into complementary DNA (cDNA) using the Fastking DNA Dispelling TRSuperMIX Reverse Transcriptase Kit (KR170801, TIANGEN, China). Quantitative real-time polymerase chain reaction was performed using the PreMix (SYBR Green) fluorescent quantitative PCR reagent kit (FP209, TIANGEN, China) on the CFX96 Real-Time PCR Detection System (Bio-Rad Laboratories, USA). The relative mRNA expression levels of *OPN3* and *VEGFR2* were calculated using the $2^{-\Delta Ct}$ or $2^{-\Delta\Delta Ct}$ method, with GAPDH serving as the internal control. The primer sequences used in this study, synthesized by Sangon Biotech (China), are provided below:

OPN3 F, 5′-CAATCCAGTGATTTATGTCTTCATGATCAGAAAG-3′,
OPN3 R, 5′-GCATTTCACTTCCAGCTGCTGGTAGGT-3′,
VEGFR2 F, 5′-GTGATTGTGGAGACTGCTGGACTG-3′,
VEGFR2 R, 5′-CTGACACATTTTGCCGCTTGGATAAC-3′,
GAPDH F, 5′-GACATCCGCAAAGACCTG-3′,
GAPDH R, 5′-GGAAGGTGGACAGCGAG-3′.

Western blot

Thirty juvenile zebrafish from each treatment group were anesthetized and euthanized on ice. The zebrafish were pooled and homogenized in RIPA lysis buffer (R0010, Solarbio, China) supplemented with 1 mM PMSF (P0100, Solarbio, China) using a tissue homogenizer (SWE-C6, Servicebio, China). For cell or zebrafish samples treated with RIPA lysis buffer, lysis was performed on ice for 30 min, followed by centrifugation to obtain protein extracts. The extracted proteins (30–200 μg) were separated via SDS-PAGE and transferred onto PVDF membranes (FFP39, Millipore, USA). The membranes were then blocked with 5% skim milk (P0216, Beyotime, China) at room temperature for 2 h and subsequently washed three times with

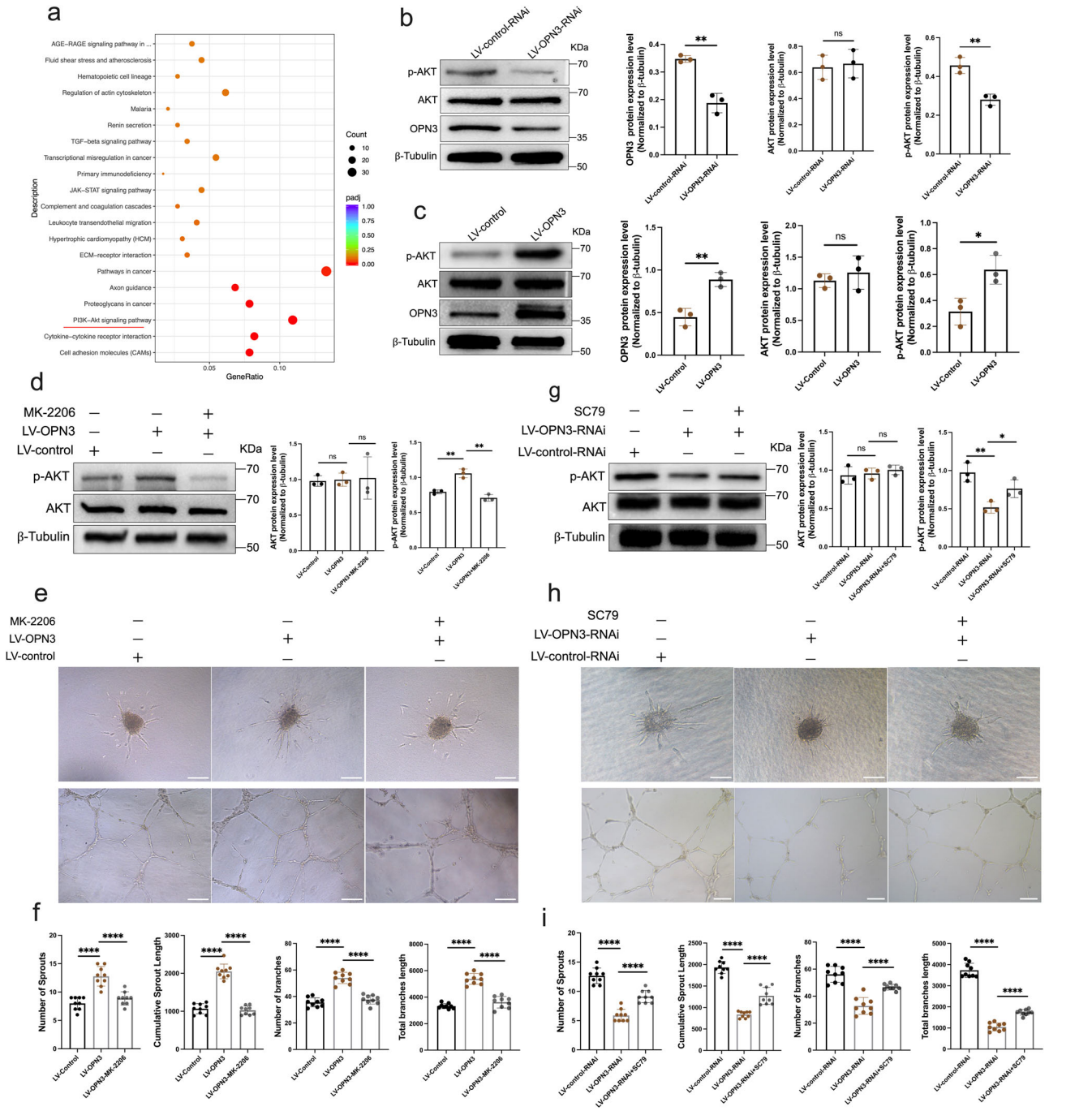

TBST (T1085, Solarbio, China). Following the washing steps, the membranes were incubated overnight at 4 °C with the following primary antibodies:

For human vascular endothelial cells:

Anti-OPN3 (ab228748, Rabbit, 1:1000, Abcam, UK)

Anti-OPN3 (A15803, Rabbit, 1:500, ABclonal, China)

Anti-VEGFR2 (55B11, Rabbit, 1:1000, Cell Signaling Technology, USA)

Anti-AKT (ABP0059, Rabbit, 1:1000, Abbkine, China)

Anti-phospho-AKT (ABP0030, Rabbit, 1:1000, Abbkine, China)

Anti-β-Tubulin (T0023, Mouse, 1:10000, Affbiotech, USA)

For zebrafish samples:

Anti-VEGFR2 (MBS8242633, Rabbit, 1:500, MyBioSource, USA)

Anti-OPN3 (A15803, Rabbit, 1:500, ABclonal, China)

Anti-phospho-AKT (4060, Rabbit, 1:2000, Cell Signaling Technology, USA)

Anti-β-Tubulin (T0034, Mouse, 1:5000, Affbiotech, USA)

After primary antibody incubation, the membranes were washed thoroughly and then incubated with HRP-conjugated secondary antibodies (Goat Anti-Rabbit IgG H&L, ab97051, 1:10000 or Goat Anti-Mouse IgG H&L, ab97023, 1:10000, Abcam, UK) for 1 h at room temperature. Protein bands were visualized using the Ultra High Sensitivity ECL Kit (HY-K1005, MedChemExpress, USA).

Chemical preparation and storage

MK-2206 (AKT inhibitor, HY-10358, MedChemExpress, USA) was also dissolved in DMSO to prepare a stock solution with a final concentration of 10 mM, stored at −80 °C for future use. For cell-based experiments,

Fig. 6 | The proangiogenic effects induced by OPN3 are possibly mediated through the promotion of AKT activation. a The scatter plot of KEGG pathway enrichment based on transcriptome sequencing results. KEGG pathway enrichment was considered significant with a threshold of *padj* < 0.05. The top 20 most significant KEGG pathways were selected for visualization in the scatter plot. The horizontal axis represents the ratio of differentially expressed genes annotated to KEGG pathways to the total number of differentially expressed genes. The vertical axis represents the KEGG pathways. The size of the dots corresponds to the number of genes annotated to the KEGG pathway, and the color gradient from red to purple reflects the significance of enrichment. The PI3K-AKT pathway was significantly enriched, as indicated by the red horizontal line. **b**, **c** Western blot analysis was used to detect the protein expression of OPN3, AKT, and p-AKT in OPN3 knockdown or overexpression HUVECs, using β-tubulin as a loading control for normalization in the WB analysis. Relative protein levels were quantified using ImageJ software ($n = 3$ independent experiments, with each experimental group consisting of 6 dishes, derived from 3 different donors, with each donor providing 2 dishes of cells). Statistical analysis was performed using an unpaired t-test: ns (not significant), $^{*}p < 0.05$, $^{**}p < 0.01$. **d** Western blot analysis was used to detect the protein levels of AKT and p-AKT in different cell groups with OPN3 overexpression or OPN3 overexpression followed by treatment with 10 μM MK-2206, using β-tubulin as a loading control for normalization in the WB analysis. Relative protein levels were quantified using ImageJ software ($n = 3$ independent experiments, with each experimental group consisting of 6 dishes, derived from 3 different donors, with each donor providing 2 dishes of cells). Statistical analysis was performed using an unpaired t-test: ns (not significant), $^{**}p < 0.01$. **e**, **f** Cells from different experimental groups were seeded on Matrigel for 10 h to record and quantify tube formation. The number and length of branches were analyzed using ImageJ software to determine the extent of tube formation. Spheroid sprouting experiments were conducted with cells from different experimental groups. The sprouts were recorded and quantified using optical microscopy, and the number and length of sprouts were analyzed using ImageJ software to evaluate the sprouting ability of HUVECs ($n = 3$ independent experiments, with each experimental group consisting of 6 dishes, derived from 3 different donors, with each donor providing 2 dishes of cells). Statistical analysis was performed using an unpaired t-test: $^{****}p < 0.0001$. The scale bar represents 100 μm. **g** Western blot analysis was used to detect the protein levels of AKT and p-AKT in different cell groups with OPN3 knockdown or OPN3 knockdown followed by treatment with 10 μM SC79, using β-tubulin as a loading control for normalization in the WB analysis. Relative protein levels were quantified using ImageJ software ($n = 3$ independent experiments, with each experimental group consisting of 6 dishes, derived from 3 different donors, with each donor providing 2 dishes of cells). Statistical analysis was performed using an unpaired t-test: ns (not significant), $^{*}p < 0.05$, $^{**}p < 0.01$. **h**, **i**. Cells from different experimental groups were seeded on Matrigel for 10 h to record and quantify tube formation. The number and length of branches were analyzed using ImageJ software to determine the extent of tube formation. Spheroid sprouting experiments were conducted with cells from different experimental groups. The tube formation was recorded and quantified using optical microscopy, and the number and length of sprouts were analyzed using ImageJ software to evaluate the sprouting ability of HUVECs ($n = 9$ dishes of cultured HUVECs from 3 different donors, with each donor replicated three times). Statistical analysis was performed using an unpaired t-test: $^{****}p < 0.0001$. The scale bar represents 100 μm. Data are presented as mean ± SEM.

HUVECs were treated with 10 μM MK-2206 for 24 h, as determined by cell viability results (Fig. S8a) and prior research findings[19,24].

SC79 (AKT agonist, HY-18749, MedChemExpress, USA) was dissolved in dimethyl sulfoxide (DMSO, D8371, Solarbio, China) to prepare a stock solution with a final concentration of 10 mM, which was stored at −80 °C until use. For cell-based experiments, HUVECs were treated with 10 μM SC79 for 24 h, a concentration determined based on cell viability results (Fig. S8b) and previous studies[55]. In the zebrafish rescue experiments, SC79 was microinjected at a concentration of 1 μM (1 nL per embryo) into fertilized eggs, which were then observed for developmental changes over 48 hpf[56,57].

VEGF (293-VE-010, R&D Systems, USA) was dissolved in phosphate-buffered saline (PBS, P1020, Solarbio, China) to achieve a stock concentration of 100 μg/mL, and the solution was stored at −80°C until required for experiments.

Cell viability assay

The effects of SC79 and MK-2206 (2HCI) at varying concentrations on HUVECs were assessed using a CCK8 assay. HUVECs were seeded into 96-well plates at a density of 1.0×10^4 cells per well. After 24 h of incubation, the cells were treated with different concentrations of SC79 (0 μM, 2.5 μM, 5 μM, 7.5 μM, 10 μM, 15 μM, and 20 μM) or MK-2206 (2HCI) (0 μM, 2.5 μM, 5 μM, 7.5 μM, 10 μM, 15 μM, and 20 μM) for 24 h. At the end of the treatment period, 10 μL of CCK8 reagent (CA1210, Solarbio, China) was added to each well, and the plates were incubated for an additional 2 h. The absorbance was then measured at 405 nm using a Multiskan SkyHigh Microplate Spectrophotometer (Thermo Fisher Scientific, USA).

SiRNA transfection

HUVECs or HDMECs were transfected with siRNA targeting *OPN3* or *VEGFR2* using Lipofectamine 2000 (Catalog No. 2097561, Invitrogen, USA) at a final siRNA concentration of 50 nM in serum-free Opti-MEM (Catalog No. 31985070, Gibco, USA). A negative control siRNA (TransheepBio, Shanghai, China) was included as a control. After 6 h of incubation, the medium was replaced with serum-containing medium to support cell growth. Silencing efficiency was evaluated by RT-qPCR 48 h post-transfection. The sequences of the siRNAs used were as follows:

OPN3: 5′-GUCACCUUUACCUUCGUGUTT-3′
VEGFR2: 5′-GGCAUGUACUGACGAUUAUUT-3′
Negative control: 5′-UUCUCCGAACGUGUCACGUTT-3′

Lentiviral infection

Lentiviral particles (Genechem, Shanghai, China) were prepared following standard protocols. These included LV-OPN3-RNAi (80513-1), LV-control-RNAi (CON313, hU6-MCS-CBh-GCGFP-IRES-puromycin), LV-OPN3 (45560-1), and LV-control (CON238, Ubi-MCS-3FLAG-SV40-EGFP-IRES-puromycin) constructs. HUVECs were seeded at a density of 1×10^5 cells per well in 12-well plates. Lentiviral particles were added to the wells at a multiplicity of infection (MOI) of 10. Once the cell confluence reached approximately 30%, the cells were infected with the lentivirus-containing medium. After 72 h of incubation, the infection medium was replaced with fresh culture medium. The cells were then maintained in culture medium supplemented with 10 μg/mL puromycin (P8230, Solarbio, China) for 1–2 weeks to select for successfully transduced cells. Puromycin-resistant colonies were subsequently collected and expanded for downstream experiments.

Plasmid transfection

Plasmids were purchased from Genechem (Shanghai, China), experiments were performed in reference to previous reports and according to the manufacturer's standard instructions[38]. The GFP-OPN3(CMV-MCS-EGFP-SV40-Neomycin) plasmid was transfected into HUVECs to up-regulate the expression of OPN3. Cells were seeded in 6 cm cell culture dishes and transfected with 3 μg/well of GFP-OPN3 plasmid and 4 μL/well of transfection reagent (R0531, Invitrogen, USA) when they reached 50% confluence. Forty-eight hours after plasmid transfection, cells were collected for subsequent experiments.

Transcriptome sequencing

RNA was extracted from HUVECs with *OPN3* knockdown and from control cells. Following extraction, the RNA underwent quality assessment to ensure integrity and purity. mRNA was subsequently enriched, and double-stranded complementary DNA (cDNA) was synthesized. Library preparation was carried out using the NEBNext® Ultra™ RNA Library Prep Kit for Illumina®, adhering to the manufacturer's protocol. The prepared libraries were sequenced on the Illumina NovaSeq 6000 platform to generate high-throughput sequencing data. After sequencing, bioinformatics analysis was performed, including data filtering to remove low-quality reads, quality control checks to ensure reliable data, and differential gene expression analysis. Further, Gene Ontology (GO) enrichment and Kyoto

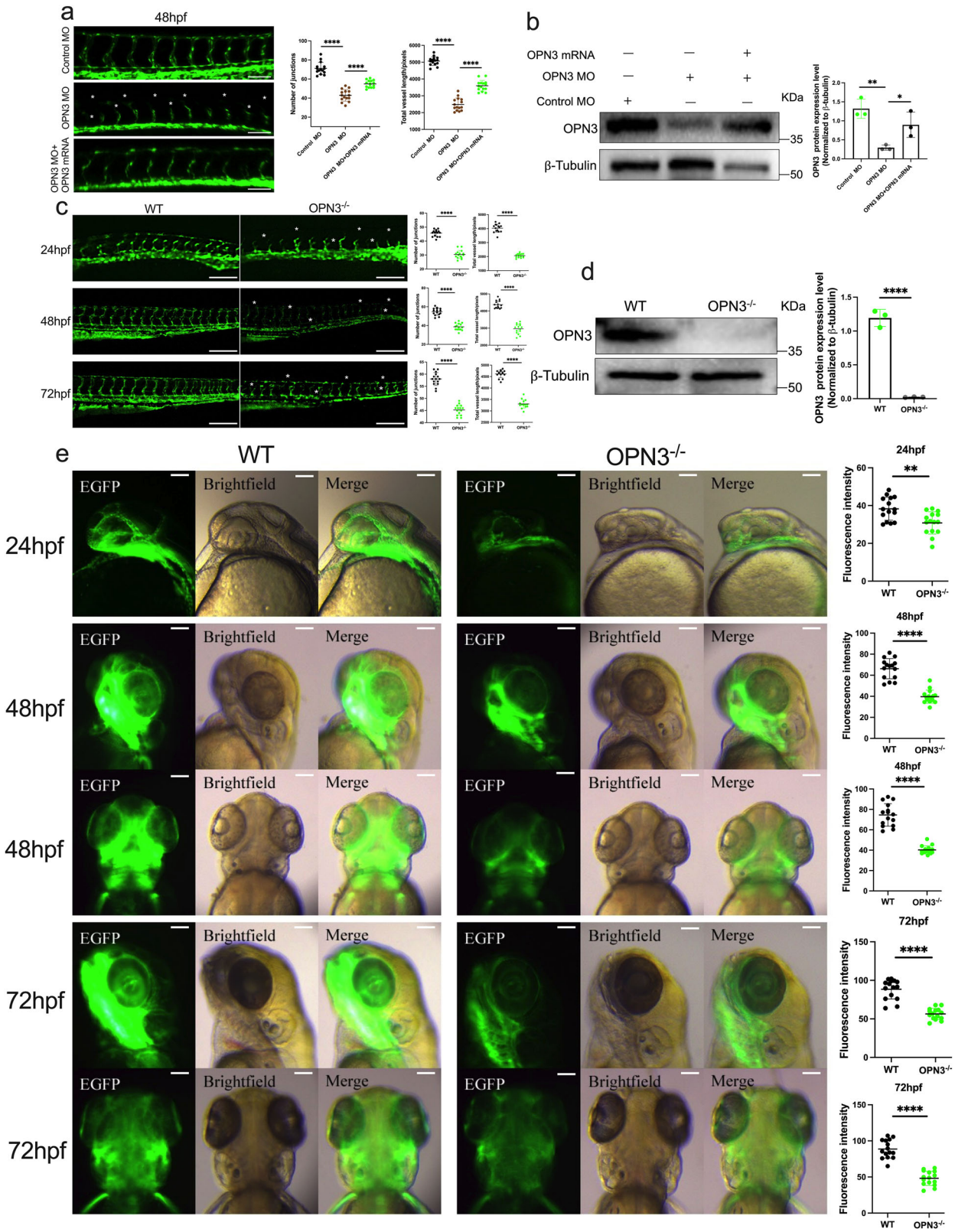

Encyclopedia of Genes and Genomes (KEGG) pathway analyses were conducted to identify functional categories and pathways associated with the differentially expressed genes (DEGs). Genes with a p-value < 0.05 were considered significantly enriched and indicative of meaningful changes in gene expression.

EdU incorporation assay

The incorporation of EdU was assessed following the manufacturer's instructions for the BeyoClick EdU Cell Proliferation Kit with Alexa Fluor 594 (C0078S, Beyotime, China). Cells were seeded at a density of 4×10^3 cells per well in 96-well plates. After 48 h of treatment, 100 μL of medium

Fig. 7 | Silencing or knockout of OPN3 causes angiogenesis deficiency during embryogenesis. a Inject *fli1*:EGFP transgenic zebrafish embryos with control MO, OPN3 MO, or OPN3 MO and OPN3 mRNA (rescue), and image the treated embryos from each group at 48 hpf using a confocal microscope. Dorsal longitudinal anastomotic vessels (DLAVs) were absent in many places (*). Intersegmental vessels (ISVs) were discontinuous, thin and short (*). The scale bar represents 100 μm. Use ImageJ to analyze the total vessel length and the number of junctions in the images from each group ($n = 15$, each individual data point represents a single zebrafish embryo). Statistical analysis was performed using an unpaired t-test: $^{****}p < 0.0001$. **b** Western blot analysis of OPN3 protein expression in *fli1*:EGFP zebrafish embryos at 48 hpf. β-tubulin was used as a loading control for normalization in the WB analysis. Relative protein levels were quantified using ImageJ ($n = 3$ batches of injected zebrafish embryos, each batch containing 30 embryos). Statistical analysis was performed using an unpaired t-test: $^{****}p < 0.0001$. **c** Confocal imaging of intersegmental vessels in wild-type (WT) sibling zebrafish embryos and OPN3 mutant zebrafish embryos ($OPN3^{-/-}$) at different developmental stages (24 hpf, 48 hpf, and 72 hpf). DLAVs were absent and discontinuous in many places (*). ISVs were discontinuous, thin and short (*). The scale bar represents 100 μm. Use ImageJ to analyze the total vessel length and the number of junctions in the images from each group ($n = 15$, each individual data point represents a single zebrafish embryo). Statistical analysis was performed using an unpaired t-test: $^{****}p < 0.0001$. **d** Western blot analysis of OPN3 protein expression in WT and $OPN3^{-/-}$ at 48 hpf. β-tubulin was used as a loading control for normalization in the WB analysis. Relative protein levels were quantified using ImageJ ($n = 3$ batches of injected zebrafish embryos, each batch containing 30 embryos). Statistical analysis was performed using an unpaired t-test: $^{****}p < 0.0001$. **e** Confocal imaging of brain vasculature in WT and $OPN3^{-/-}$ at different developmental stages (24 hpf, 48 hpf, and 72 hpf). The scale bar represents 100 μm. Use ImageJ to analyze the fluorescence intensity in the images from each group ($n = 15$, each individual data point represents the trunk or brain region of a single zebrafish embryo). Statistical analysis was performed using an unpaired t-test: $^{**}p < 0.01$, $^{****}p < 0.0001$. Data are presented as mean ± SEM.

containing 50 μM EdU was added to each well, and the cells were incubated for 2 h. Subsequently, the cells were fixed with 4% paraformaldehyde in PBS for 15 min, permeabilized with 0.5% Triton X-100 in PBS for 10 min, and subjected to the Click reaction according to the kit protocol. The nuclei were counterstained with Hoechst 33342. Fluorescence microscopy was used to visualize and quantify EdU-positive nuclei.

Flow cytometry

HDMECs were collected by centrifugation, and the resulting cell pellet was resuspended in flow cytometry buffer to achieve a concentration of 1×10^6 cells per 100 μL. To prevent non-specific binding, 10% goat serum (Absin, abs993, China) was added to the suspension, which was then incubated for 15 min at room temperature. Afterward, anti-CD31 antibody (1:20 dilution, Mouse, ab9498, Abcam, UK) was added, and the mixture was incubated at 4 °C in the dark for 30 min with gentle mixing. Following two washes with flow cytometry buffer, cells were incubated with Goat Anti-Mouse IgG H&L (Alexa Fluor® 647, ab150115, 1:2000 dilution, Abcam, UK) for 30 min at 4 °C in the dark. The cells were then washed twice more and analyzed by flow cytometry (BD Biosciences, USA) to determine the proportion of CD31-positive cells. The data were processed using FlowJo software (v10.10, USA).

For HUVECs, the cells were collected, washed with precooled PBS, and fixed overnight with 70% ethanol at 4 °C, following the instructions provided in the Cell Cycle Detection kit (C1052-7, Beyotime, China). After centrifugation and PBS washes, RNAse solution (100 μg/mL) was added and incubated at 37 °C for 30 min. Next, propidium iodide (50 μg/mL) was added, and the cells were incubated at 4 °C for at least 30 min in the dark. At least 10,000 cells were analyzed using a flow cytometer, and FlowJo (v10.10, USA) or ModFit LT (v5.0, USA) software was employed to determine the percentage of cells in different phases of the cell cycle (G1, S, and G2).

Transwell assay

HUVECs, treated with various experimental conditions, were suspended in serum-free medium and seeded into the upper chambers of Transwell plates (3422, Corning, USA) with a pore size of 0.8 μm at a density of 1×10^4 cells per 200 μL of medium. Complete medium (400 μL) containing 10% FBS was added to the lower chambers. After 24 h of incubation, the medium in the upper chambers was removed. Cells that had migrated through the membrane were fixed with 4% paraformaldehyde for 15 min, stained with 0.1% crystal violet for 10 min, and then observed under a light microscope (Nikon, Japan). Images were captured and recorded for analysis.

Tube formation assay

The ECs tube formation assay is one of the most widely used and reliable methods for studying angiogenesis in vitro. Following previously reported protocols and kit instructions[58], the ECMatrix solution (ECM625, Sigma-Aldrich, USA) was mixed with a 10× dilution buffer in a ratio of 9:1. A total of 50 μL of the mixture was added to a 96-well tissue culture plate. After incubation at 37 °C for 1 h to allow the mixture to solidify, 1×10^4 cells/100 μL were seeded onto the surface of the gel. The cells were then incubated at 37 °C for 10 h, and tube formation was observed under an inverted optical microscope. The cells were fixed with 4% paraformaldehyde, and images were captured for documentation. Image analysis was performed using the angiogenesis plug-in of ImageJ.

Spheroid-based sprouting angiogenesis assay

The sphere-based sprouting assay is a well-established and reliable method for studying angiogenesis in vitro[59]. Begin by carefully mixing 4 mL of cell culture medium containing 8×10^4 cells with 1 mL of methylcellulose solution (M0512, Sigma-Aldrich, USA) at a concentration of 12 mg/mL. Next, pipette 25 μL of the cell mixture onto the lid of a 10 cm square Petri dish (688102, Greiner Bio One International, Austria). Incubate the dish upside down in a humidified incubator for 24 h to allow the formation of spheroid structures. After incubation, gently rinse the hanging drops with PBS and resuspend the HUVECs in 2 mL of a 20% FBS-containing methylcellulose solution. Then, add 0.25 mL of ten-fold diluted Medium 199 (M0650, Sigma-Aldrich, USA) to 2 mL of rat type I collagen solution (35436, Corning, USA) and mix thoroughly. Afterward, transfer the spheroid-collagen mixture into a 12-well plate and incubate at 37 °C with 5% CO_2 for 30 min to allow the collagen to gel. Following this, introduce 25 ng/mL of VEGF (293-VE-010, R&D Systems, USA) and continue incubation for an additional 24 h. Finally, capture images of the samples under a microscope. Image analysis: Quantifying the sprout length of all sprouts in the spheroid using ImageJ software.

Immunoprecipitation

Protein A/G magnetic beads (20 μL, P2179S, Beyotime, China) were incubated with primary antibodies for 1.5 h, and the supernatant was removed according to the instructions provided with the immunoprecipitation kit (P2179S, Beyotime, China). Cell lysates were prepared by homogenizing 500 μL of lysis buffer (containing 5 μL of protease inhibitor cocktail). The lysates were then centrifuged at 15,000 rpm for 15 min at 4 °C to remove cell debris, and the resulting supernatant was divided into Input, IgG, and IP fractions. The IP fraction was mixed with antibody-bound beads and incubated overnight at 4 °C. The following primary antibodies were used: anti-IgG (P2179S, Rabbit, 1:100, Beyotime, China), anti-VEGFR2 (55B11, Rabbit, 1:100, Cell Signaling Technology, USA), and anti-OPN3 (A15803, Rabbit, 1:100, ABclonal, China)[36]. After washing the beads three times with lysis buffer, 100 μL of SDS-PAGE loading buffer was added, and the samples were heated at 95 °C for 5 min. Protein analysis was performed by Western blotting using primary antibodies against VEGFR2 (55B11, Rabbit, 1:1000, Cell Signaling Technology, USA) and OPN3 (A15803, Rabbit, 1:500, ABclonal, China). The primary antibody is detected by incubation with the universal secondary antibody (heavy chain + light chain, M21008, 1:2000, Abmart, China).

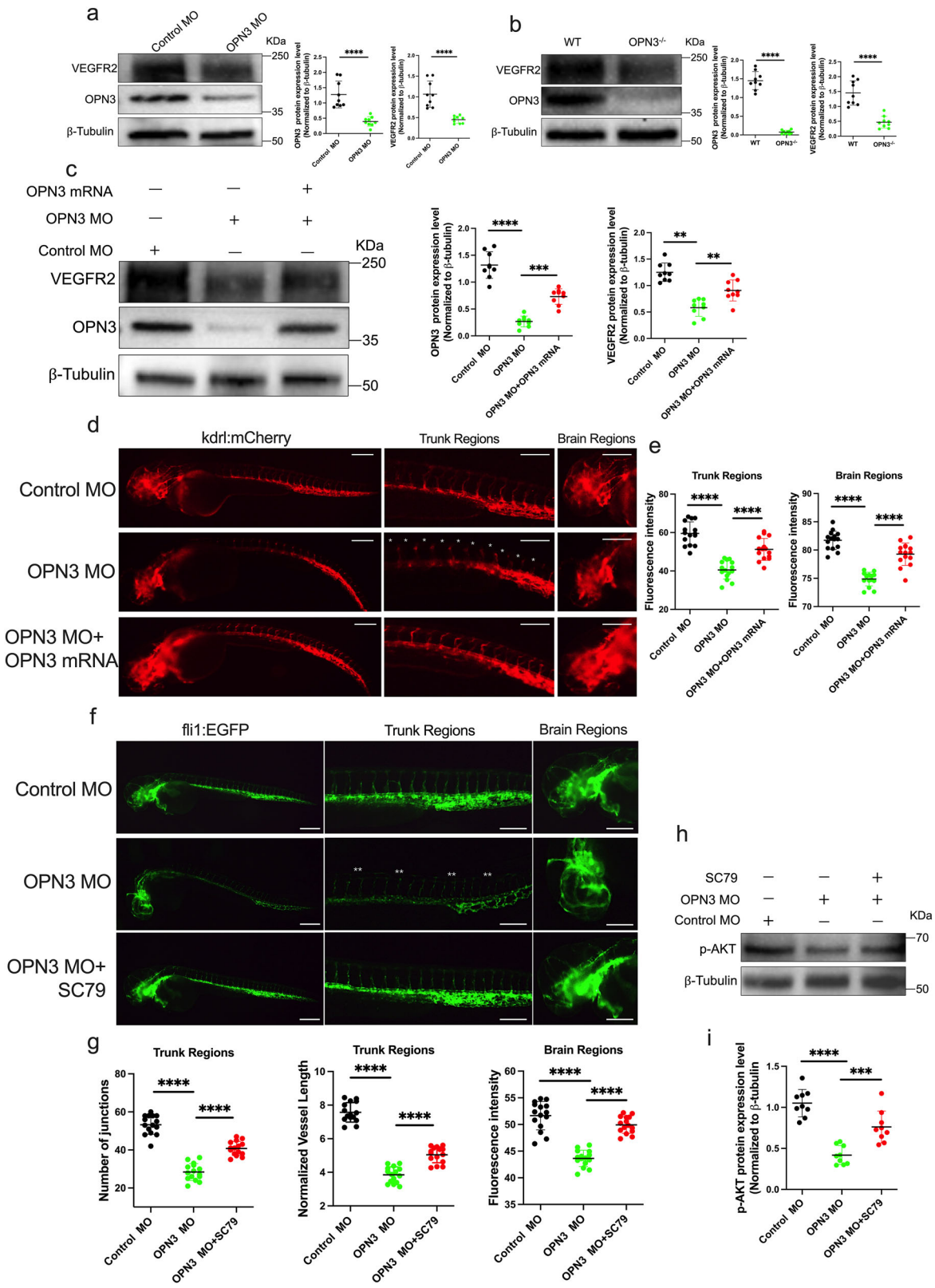

Molecular docking

The OPN3 protein structure was predicted using AlphaFold2 (https://alphafold.ebi.ac.uk/entry/Q9H1Y3), while the VEGFR2 structure was obtained from the PDB database (ID: 3KVQ). Protonation at neutral pH (7.0) was performed using the H++3 online server. Heteroatoms and water molecules were removed using UCSF Chimera, leaving only the protein structure and assigning the Amber14SB force field charges. Protein-protein docking was performed using HDOCK with the ITScorePP scoring function. Out of 100 output configurations, the top 10 were selected based on their docking and confidence scores, and the configuration with the highest scores was chosen for further analysis. PyMOL2.04 was used for 3D visualization, while Maestro (academic version) was employed for 2D interaction analysis, including statistical evaluation of interaction types, distances, and quantities.

Fig. 8 | OPN3 regulates VEGFR2 expression and AKT activation in vivo. **a** Western blot analysis of OPN3 and VEGFR2 protein expression in *fli1*:EGFP zebrafish embryos after OPN3 knockdown using MO. β-tubulin was used as a loading control for normalization in the WB analysis. Relative protein levels were quantified using ImageJ ($n = 9$ batches of injected zebrafish embryos, each batch containing 30 embryos). Statistical analysis was performed using an unpaired t-test: $^{****}p < 0.0001$. **b** Western blot analysis of OPN3 and VEGFR2 protein expression in WT and OPN3$^{-/-}$ at 48 hpf. β-tubulin was used as a loading control for normalization in the WB analysis. Relative protein levels were quantified using ImageJ ($n = 9$ batches of injected zebrafish embryos, each batch containing 30 embryos). Statistical analysis was performed using an unpaired t-test: $^{****}p < 0.0001$. **c** Western blot analysis of OPN3 and VEGFR2 protein expression in *kdrl*:mCherry zebrafish embryos after OPN3 knockdown using MO, and after co-injection of OPN3 MO with OPN3 mRNA. β-tubulin was used as a loading control for normalization in the WB analysis. Relative protein levels were quantified using ImageJ ($n = 9$ batches of injected zebrafish embryos, each batch containing 30 embryos). Statistical analysis was performed using an unpaired t-test: $^{**}p < 0.01$, $^{***}p < 0.001$, $^{****}p < 0.0001$. **d** Inject *kdrl*:mCherry transgenic zebrafish embryos with Control MO, OPN3 MO, or OPN3 MO and OPN3 mRNA, and image the treated embryos from each group at 48 hpf using a confocal microscope. The fluorescence of kdrl is absent and discontinuous in many places (*). **e** Use ImageJ to analyze the fluorescence intensity in the images from each group ($n = 15$, each individual data point represents the trunk or brain region of a single zebrafish embryo). Statistical analysis was performed using an unpaired t-test: $^{****}p < 0.0001$. The scale bar represents 100 μm. **f** Inject *fli1*:EGFP transgenic zebrafish embryos with Control MO, OPN3 MO, or OPN3 MO and SC79, and image the treated embryos from each group at 48 hpf using a confocal microscope. DLAVs and ISVs were absent and discontinuous in many places (**). **g** Use ImageJ to analyze the normalized vessel length and the number of junctions in the images from each group ($n = 15$, each individual data point represents the trunk or brain region of a single zebrafish embryo). Statistical analysis was performed using an unpaired t-test: $^{****}p < 0.0001$. The scale bar represents 100 μm. **h** Western blot analysis of p-AKT protein expression in *fli1*:EGFP zebrafish embryos after OPN3 knockdown using MO, and after co-injection of OPN3 MO with SC79. β-tubulin was used as a loading control for normalization in the WB analysis. **i** Relative protein levels were quantified using ImageJ ($n = 9$ batches of injected zebrafish embryos, each batch containing 30 embryos). Statistical analysis was performed using an unpaired t-test: $^{***}p < 0.001$, $^{****}p < 0.0001$. Data are presented as mean ± SEM.

Zebrafish and Morpholinos

Adult zebrafish Tg(*fli1*:EGFP) and Tg(*kdrl*:mCherry) lines were obtained from the China Zebrafish Resource Center and maintained at 28 °C under a 14 h light/10 h dark cycle. At the 1-cell stage, embryos were microinjected with 8 ng of morpholino oligonucleotides (Gene Tools, USA). The sequences of the morpholinos were as follows:

OPN3 morpholino: AAGACATGGACTTACCATTTTAACT; Mismatch control morpholino: CCTCTTACCTCAGTTACAATTTATA. For rescue experiments, the T7-OPN3-mCherry plasmids were linearized using Eco1471 (Thermo Fisher Scientific, USA), and capped mRNAs were synthesized using the mMESSAGE mMACHINE™ T7 Ultra Transcription Kit (Ambion, USA) according to the manufacturer's instructions. The synthesized *OPN3* mRNA was diluted to a final concentration of 100 ng/μL, and 1 nL of the mRNA solution was microinjected into the embryos at the 1-cell stage. For imaging, embryos were carefully mounted in 1.0% low-melting-point agarose to minimize movement during observation. Fluorescent signals were observed using an Olympus FV1000-MPE confocal microscope to monitor the effects of morpholino injection and mRNA rescue on vascular development. We have complied with all relevant ethical regulations for animal use. All experimental procedures were approved by the Institutional Animal Care and Use Committee of Guizhou Medical University (Approval #: #2403615) and were carried out in compliance with the ethical guidelines set forth by the China Academy of Food and Drug Inspection and Quarantine.

Zebrafish OPN3 knockout

Based on previous studies, we used the CRISPR/Cas9 system to knock out the *OPN3* gene[60]. The genomic DNA sequence of *OPN3* was retrieved from the NCBI database, focusing on the exonic regions to design specific sgRNA sequences targeting the *OPN3* gene. Following standard protocols, zebrafish fertilized eggs were collected, and the sgRNA was synthesized to a final concentration of approximately 200 ng/μL. The Cas9 protein was prepared at a final concentration of 400 ng/μL. The sgRNA and Cas9 protein mixture was then microinjected into the one-cell stage zebrafish embryos at a total injection volume of 1 nL per embryo. After injection, the embryos were incubated and allowed to develop until 24 hpf. At 24 hpf, five embryos from each experimental group were randomly selected, and genomic DNA was extracted from each embryo. The PCR products were then sequenced to detect sgRNA activity. Based on the mutation peaks, the F0 generation was bred to sexual maturity and crossed with wild-type fish to obtain F1 embryos. The F1 embryos were raised to sexual maturity, and part of the tail fin tissue was collected for PCR amplification and sequencing to confirm the mutation genotype. F1 individuals with the same genotype for the allele mutation (both males and females) were then mated to produce F2 generation offspring. Homozygous *OPN3*$^{-/-}$ zebrafish were identified in the F2 generation and used for subsequent analysis. The CRISPR sequence was designed as follows: CCTGCTGGTGTCCCTGACTGGGG

The PCR amplification and sequencing primers were designed as follows:

OPN3-F1: 5′-GAAGCTCTCTTGTGGATCCG-3′
OPN3-R1: 5′-AAACGCGTAAATATATGCGC-3′
GADPH-F1: 5′- CCAACTGCCTGGCTCCTT-3′
GADPH-R1: 5′- CCCATCAACGGTCTTCTGTG-3′
OPN3-seqF: 5′-GAATCGGGTCACTCACTTT-3′

Computer analysis of the vasculature and fluorescence intensity was performed using ImageJ with the following plugins: Skeletonize (2D/3D) and Analyze Skeleton for vasculature analysis, and Measure RGB for fluorescence intensity, respectively.

Fluorescence intensity measurement and co-localization analysis

To quantitatively analyze fluorescence intensity in zebrafish and HUVECs, fluorescence microscopy images were processed using ImageJ and the Measure RGB plugin. Regions of interest (ROIs) were selected, and mean intensity values for red, green, and blue channels were measured. Background intensity from a non-fluorescent region was subtracted to correct for nonspecific signals, and the average intensity was used for statistical analysis.

For co-localization analysis of two fluorescently labeled molecules in HUVECs, fluorescence images were analyzed using ImageJ and the Coloc 2 plugin. The green and red channels were separated, ROIs were selected, and Manders' coefficients (tM1 and tM2) were used to quantify co-localization. Background correction was applied, and co-localization percentages were calculated. Intensity profiles were extracted using the "Plot Profile" function, and numerical data were exported for further analysis.

Statistics and reproducibility

Statistical analyses were performed using GraphPad Prism (version 10.4.1). Data are presented as mean ± SEM. An unpaired t-test was used to compare groups, with significance levels set at $^{*}p < 0.05$, $^{**}p < 0.01$, $^{***}p < 0.001$, and $^{****}p < 0.0001$, as specified in the figure legends. For all in vitro experiments, at least 3 different donors were used for each experimental. For in vivo experiments, at least 15 zebrafish embryos were analyzed for each experimental group. The sample size for each experiment is indicated in the figure legends.

Reporting summary

Further information on research design is available in the Nature Portfolio Reporting Summary linked to this article.

Data availability

All data generated during our study are fully documented in the published article and its Supplementary Information. The RNA-seq data generated in this study have been deposited in the NCBI Sequence Read Archive (SRA) under the accession number PRJNA1234294. Source data for graphs are provided in the Supplementary Data of this article. The gating strategy for all FACS plots is presented in Supplementary Information (Fig. S10). All original Western blot images are available in Supplementary Information (Fig. S11). All other data supporting the findings of this study are available from the corresponding author upon reasonable request.

Received: 3 June 2024; Accepted: 19 March 2025;
Published online: 31 March 2025

References

1. Carmeliet, P. Mechanisms of angiogenesis and arteriogenesis. *Nat. Med* **6**, 389–395 (2000).
2. Carmeliet, P. Angiogenesis in life, disease and medicine. *Nature* **438**, 932–936 (2005).
3. Ferrara, N. & Kerbel, R.S. Angiogenesis as a therapeutic target. *Nature* **438**, 967–974 (2005).
4. Holmes, K., Roberts, O.L., Thomas, A.M. & Cross, M.J. Vascular endothelial growth factor receptor-2: structure, function, intracellular signalling and therapeutic inhibition. *Cell Signal* **19**, 2003–2012 (2007).
5. Wang, X., Bove, A.M., Simone, G. & Ma, B. Molecular Bases of VEGFR-2-Mediated Physiological Function and Pathological Role. *Front Cell Dev. Biol.* **8**, 599281 (2020).
6. Kilpatrick, L.E. & Hill, S.J. Transactivation of G protein-coupled receptors (GPCRs) and receptor tyrosine kinases (RTKs): Recent insights using luminescence and fluorescence technologies. *Curr. Opin. Endocr. Metab. Res* **16**, 102–112 (2021).
7. Cui, H. et al. GPR126 protein regulates developmental and pathological angiogenesis through modulation of VEGFR2 receptor signaling. *J. Biol. Chem.* **289**, 34871–34885 (2014).
8. Tsopanoglou, N.E. & Maragoudakis, M.E. On the mechanism of thrombin-induced angiogenesis. Potentiation of vascular endothelial growth factor activity on endothelial cells by up-regulation of its receptors. *J. Biol. Chem.* **274**, 23969–23976 (1999).
9. Kilpatrick, L. E. et al. Complex Formation between VEGFR2 and the β2-Adrenoceptor. *Cell Chem Biol* **26** https://doi.org/10.1016/j.chembiol.2019.02.014 (2019).
10. Parker, S.L., Parker, M.S., Sah, R. & Sallee, F. Angiogenesis and rhodopsin-like receptors: a role for N-terminal acidic residues?. *Biochem Biophys. Res Commun.* **335**, 983–992 (2005).
11. Shichida, Y. & Matsuyama, T. Evolution of opsins and phototransduction. *Philos. Trans. R. Soc. Lond. B Biol. Sci.* **364**, 2881–2895 (2009).
12. Terakita, A. The opsins. *Genome Biol.* **6**, 213 (2005).
13. Nguyen, M.-T.T. et al. An opsin 5-dopamine pathway mediates light-dependent vascular development in the eye. *Nat. cell Biol.* **21**, 420–429 (2019).
14. Rao, S. et al. A direct and melanopsin-dependent fetal light response regulates mouse eye development. *Nature* **494**, 243–246 (2013).
15. Sikka, G. et al. Melanopsin mediates light-dependent relaxation in blood vessels. *Proc. Natl Acad. Sci. USA* **111**, 17977–17982 (2014).
16. Barreto Ortiz, S. et al. Opsin 3 and 4 mediate light-induced pulmonary vasorelaxation that is potentiated by G protein-coupled receptor kinase 2 inhibition. *Am. J. Physiol. Lung Cell Mol. Physiol.* **314** https://doi.org/10.1152/ajplung.00091.2017 (2018).
17. Trimm, E. & Red-Horse, K. Vascular endothelial cell development and diversity. *Nat. Rev. Cardiol.* **20**, 197–210 (2023).
18. Pusztaszeri, M.P., Seelentag, W. & Bosman, F.T. Immunohistochemical expression of endothelial markers CD31, CD34, von Willebrand factor, and Fli-1 in normal human tissues. *J. Histochem Cytochem* **54**, 385–395 (2006).
19. Lan, Y. et al. Opsin 3 mediates UVA-induced keratinocyte supranuclear melanin cap formation. *Commun. Biol.* **6**, 238 (2023).
20. Yan, Y., Zhang, D., Zhou, P., Li, B. & Huang, S.-Y. HDOCK: a web server for protein-protein and protein-DNA/RNA docking based on a hybrid strategy. *Nucleic Acids Res* **45**, W365–W373 (2017).
21. Shinkai, A. et al. Mapping of the sites involved in ligand association and dissociation at the extracellular domain of the kinase insert domain-containing receptor for vascular endothelial growth factor. *J. Biol. Chem.* **273**, 31283–31288 (1998).
22. Koch, S. & Claesson-Welsh, L. Signal transduction by vascular endothelial growth factor receptors. *Cold Spring Harb. Perspect. Med* **2**, a006502 (2012).
23. Shiojima, I. & Walsh, K. Role of Akt signaling in vascular homeostasis and angiogenesis. *Circ. Res* **90**, 1243–1250 (2002).
24. Liu, R. et al. The Akt-specific inhibitor MK2206 selectively inhibits thyroid cancer cells harboring mutations that can activate the PI3K/Akt pathway. *J. Clin. Endocrinol. Metab.* **96**, E577–E585 (2011).
25. Jo, H. et al. Small molecule-induced cytosolic activation of protein kinase Akt rescues ischemia-elicited neuronal death. *Proc. Natl Acad. Sci. USA* **109**, 10581–10586 (2012).
26. Vogel, A.M. & Weinstein, B.M. Studying vascular development in the zebrafish. *Trends Cardiovasc Med* **10**, 352–360 (2000).
27. Lawson, N.D. & Weinstein, B.M. In vivo imaging of embryonic vascular development using transgenic zebrafish. *Dev. Biol.* **248**, 307–318 (2002).
28. Wang, Y. et al. Moesin1 and Ve-cadherin are required in endothelial cells during in vivo tubulogenesis. *Dev. (Camb., Engl.)* **137**, 3119–3128 (2010).
29. Carmeliet, P. Angiogenesis in health and disease. *Nat. Med.* **9**, 653–660 (2003).
30. Carmeliet, P. & Jain, R.K. Angiogenesis in cancer and other diseases. *Nature* **407**, 249–257 (2000).
31. Ferrara, N., Gerber, H.-P. & LeCouter, J. The biology of VEGF and its receptors. *Nat. Med* **9**, 669–676 (2003).
32. Chakraborty, M.P., et al. Molecular basis of VEGFR1 autoinhibition at the plasma membrane. *Nat. Commun.* **15**, 1346 (2024).
33. Shibuya, M. Differential roles of vascular endothelial growth factor receptor-1 and receptor-2 in angiogenesis. *J. Biochem Mol. Biol.* **39**, 469–478 (2006).
34. Cao, Y. Positive and negative modulation of angiogenesis by VEGFR1 ligands. *Sci. Signal* **2**, re1 https://doi.org/10.1126/scisignal.259re1 (2009).
35. Shibuya, M. Vascular endothelial growth factor and its receptor system: physiological functions in angiogenesis and pathological roles in various diseases. *J. Biochem* **153**, 13–19 (2013).
36. Ozdeslik, R.N., Olinski, L.E., Trieu, M.M., Oprian, D.D. & Oancea, E. Human nonvisual opsin 3 regulates pigmentation of epidermal melanocytes through functional interaction with melanocortin 1 receptor. *Proc. Natl Acad. Sci. USA* **116**, 11508–11517 (2019).
37. Haddad, H.K., et al. Hypothalamic opsin 3 suppresses MC4R signaling and potentiates Kir7.1 to promote food consumption. *Proc. Natl Acad. Sci. USA* **122**, e2403891122 (2025).
38. Dong, X. et al. OPN3 Regulates Melanogenesis in Human Congenital Melanocytic Nevus Cells through Functional Interaction with BRAF(V600E). *J. Invest Dermatol* **142**, 3020–3029.e3025 (2022).
39. Hyde, C.A.C. et al. Targeting extracellular domains D4 and D7 of vascular endothelial growth factor receptor 2 reveals allosteric receptor regulatory sites. *Mol. Cell Biol.* **32**, 3802–3813 (2012).
40. King, C., Wirth, D., Workman, S. & Hristova, K. Cooperative interactions between VEGFR2 extracellular Ig-like subdomains ensure VEGFR2 dimerization. *Biochim Biophys. Acta Gen. Subj.* **1861**, 2559–2567 (2017).
41. Sarabipour, S., Ballmer-Hofer, K. & Hristova, K. VEGFR-2 conformational switch in response to ligand binding. *Elife* **5**, e13876 (2016).

42. Yang, Y., Xie, P., Opatowsky, Y. & Schlessinger, J. Direct contacts between extracellular membrane-proximal domains are required for VEGF receptor activation and cell signaling. *Proc. Natl Acad. Sci. USA* **107**, 1906–1911 (2010).
43. Koyanagi, M., Takada, E., Nagata, T., Tsukamoto, H. & Terakita, A. Homologs of vertebrate Opn3 potentially serve as a light sensor in nonphotoreceptive tissue. *Proc. Natl Acad. Sci. USA* **110**, 4998–5003 (2013).
44. Bai, C.-W. et al. G protein subunit alpha i2's pivotal role in angiogenesis. *Theranostics* **14**, 2190–2209 (2024).
45. Sun, J. et al. Gαi1 and Gαi3mediate VEGF-induced VEGFR2 endocytosis, signaling and angiogenesis. *Theranostics* **8**, 4695–4709 (2018).
46. Zhou, X.E., Melcher, K. & Xu, H.E. Structure and activation of rhodopsin. *Acta Pharm. Sin.* **33**, 291–299 (2012).
47. Yamashita, T., Terakita, A. & Shichida, Y. Distinct roles of the second and third cytoplasmic loops of bovine rhodopsin in G protein activation. *J. Biol. Chem.* **275**, 34272–34279 (2000).
48. Okada, T., Ernst, O.P., Palczewski, K. & Hofmann, K.P. Activation of rhodopsin: new insights from structural and biochemical studies. *Trends Biochem Sci.* **26**, 318–324 (2001).
49. Scheerer, P. et al. Crystal structure of opsin in its G-protein-interacting conformation. *Nature* **455**, 497–502 (2008).
50. Dungel, P. et al. Low level light therapy by LED of different wavelength induces angiogenesis and improves ischemic wound healing. *Lasers Surg. Med.* **46**, 773–780 (2014).
51. Guido, M.E. et al. Non-visual Opsins and Novel Photo-Detectors in the Vertebrate Inner Retina Mediate Light Responses Within the Blue Spectrum Region. *Cell Mol. Neurobiol.* **42**, 59–83 (2022).
52. Castellano-Pellicena, I. et al. Does blue light restore human epidermal barrier function via activation of Opsin during cutaneous wound healing?. *Lasers Surg. Med.* **51**, 370–382 (2019).
53. Regazzetti, C. et al. Melanocytes Sense Blue Light and Regulate Pigmentation through Opsin-3. *J. investigative Dermatol.* **138**, 171–178 (2018).
54. Jaffe, E.A., Nachman, R.L., Becker, C.G. & Minick, C.R. Culture of human endothelial cells derived from umbilical veins. Identification by morphologic and immunologic criteria. *J. Clin. Invest* **52**, 2745–2756 (1973).
55. Xu, T.-Y. et al. Metrnl deficiency retards skin wound healing in mice by inhibiting AKT/eNOS signaling and angiogenesis. *Acta Pharm. Sin.* **44**, 1790–1800 (2023).
56. Jiang, Y., Zhao, X., Chen, J., Aniagu, S. & Chen, T. PM2.5 induces cardiac malformations via PI3K/akt2/mTORC1 signaling pathway in zebrafish larvae. *Environ. Pollut. (Barking, Essex: 1987)* **323**, 121306 (2023).
57. Shen, Y.-J., Chen, H.-Y., Chang, C.-W., Huang, Y.-C. & Cheng, Y.-C. Chemical modulation of Akt signaling enhances spinal cord regeneration in zebrafish. *Brain Res* **1846**, 149248 (2025).
58. Kelley, M., Fierstein, S., Purkey, L. & DeCicco-Skinner, K. Endothelial Cell Tube Formation Assay: An In Vitro Model for Angiogenesis. *Methods Mol. Biol.* **2475**, 187–196 (2022).
59. Tetzlaff, F. & Fischer, A. Human Endothelial Cell Spheroid-based Sprouting Angiogenesis Assay in Collagen. *Bio Protoc.* **8**, e2995 (2018).
60. Medishetti, R., et al. CRISPR-Cas9-induced gene knockout in zebrafish. *STAR Protoc.* **3**, 101779 (2022).

Acknowledgements

This study was supported by the National Natural Science Foundation of China (grant numbers 82360617, 82260615, 82173397, 82360458, 82404116), and Foundation of Guizhou Medical University Key Laboratory of Dermato-photomedicine ([2024]fy005).

Author contributions

H. Lu. and H. Luo: designed the experimental protocol. H. Luo: carried out the experiments. H. Luo and W. Zhang: wrote the main manuscript text, prepared figures, and revised the manuscript. W. Zeng, Y. Wang and J. Feng.: Date analyses. Y. Lan., X.Dong., T. Liu. and Y. Sun.: Experimental technical support. All authors reviewed the manuscript.

Competing interests

The authors declare no competing interests.

Ethics approval and consent to participate

All donors provided informed written consent before participation in this study. The study was approved by the Ethics Committee of the Affiliated Hospital of Guizhou Medical University (Approval: #2021-541; #2023-740). Animal procedures were approved by the Institutional Animal Care and Use Committee of Guizhou Medical University (Approval #: #2403615) and were carried out in compliance with the ethical guidelines set forth by the China Academy of Food and Drug Inspection and Quarantine.

Additional information

Supplementary information The online version contains supplementary material available at https://doi.org/10.1038/s42003-025-07958-4.

Correspondence and requests for materials should be addressed to Hongguang Lu.

Peer review information *Communications Biology* thanks Sujata Rao and the other, anonymous, reviewer(s) for their contribution to the peer review of this work. Primary Handling Editors: Kaliya Georgieva. A peer review file is available.